Lithos 119 (2010) 147–161

Contents lists available at ScienceDirect

Lithos

journal homepage: www.elsevier.com/locate/lithos

Origin of extremely PGE-rich mafic magma system: An example from the Jinbaoshan ultramafic sill, Emeishan large igneous province, SW China

Christina Yan Wang [a,*], Mei-Fu Zhou [b], Liang Qi [c]

[a] Guangzhou Institute of Geochemistry, Chinese Academy of Sciences, Guangzhou 510640, China
[b] Department of Earth Sciences, The University of Hong Kong, Hong Kong, China
[c] State Key Lab of Ore Deposit Geochemistry, Institute of Geochemistry, Chinese Academy of Sciences, Guiyang 550002, China

ARTICLE INFO

Article history:
Received 6 December 2009
Accepted 23 July 2010
Available online 1 August 2010

Keywords:
Platinum-group elements (PGE)
PGE-rich horizons
Sulfide saturation
The Jinbaoshan sill
SW China

ABSTRACT

The ~260 Ma Jinbaoshan sill is part of the Permian Emeishan large igneous province in SW China and is mainly composed of wehrlite and hosts a PGE deposit containing ~45 tonnes of Pt and Pd with ore grades ranging from 1 to 5 ppm Pt + Pd. The sill is composed of several PGE-rich horizons at different stratigraphic heights. A ~5 m-thick PGE-rich horizon at the base of the sill, which is underlain by a chromite-rich, PGE-poor layer, accounts for 44% of the total ore reserve.

The Jinbaoshan sill is rich in PGEs with Ir ranging from 1.7 to 138 ppb, Ru from 0.9 to 39 ppb, Rh from 3.1 to 133 ppb, and a total Pt and Pd from 76 to 5371 ppb. All the rocks from the sill display primitive mantle-normalized chacophile element patterns enriched in PGEs relative to Ni and Cu. The low Cu/Pd ratios (20 to 1938) of the rocks relative to the primitive mantle (Cu/Pd = 7000) imply that there was no sulfide fractionation of the magmas. The PGE enrichment of the sill indicates that it formed from extremely PGE-rich magmas. Modeling results show that such PGE-rich magmas likely resulted from a multistage-dissolution upgrading process in an open magma conduit system.

Large amounts of chromite crystallization triggered sulfide saturation when PGE-rich magmas emplaced into the upper magma chamber of the system. Settling and sorting of chromite and most sulfide liquids along with olivine resulted in the formation of the largest PGE-rich horizon at the base of the sill. The rest minor sulfide liquid accumulated to form PGE-rich horizons in the middle part of the sill aided by turbulence and convection within the magma chamber.

1. Introduction

Magmatic sulfide deposits include Ni–Cu-dominant and sulfide-rich (20–90% sulfide) deposits and PGE-dominant and sulfide-poor (0.5–5% sulfide) deposits (Naldrett, 2004). Typical examples of Ni–Cu-dominant sulfide deposits are those in Noril'sk, Russia (Naldrett et al., 1995), Jinchuan, NW China (Chai and Naldrett, 1992a,b), Uitkomst, South Africa (Gauert et al., 1995) and Voisey's Bay, Canada (Li and Naldrett, 1999). These deposits tend to occur in small magma conduit systems where the enhanced ore potentials are attributed to upgrading of precipitated sulfides by reacting with multiple flows of undepleted magma using the same conduit (Maier et al., 2001). Most of the PGE-dominant deposits are hosted in layered intrusions, such as the Bushveld and Stillwater Complexes and the Great Dyke (Naldrett, 2004). Within these layered intrusions, very PGE-rich sulfides occur at specific horizons, either with or without associated chromitite, such as the chromite layers of the Merensky Reef (Barnes and Maier, 2002; Godel et al., 2007) and UG-2 of the Bushveld Complex (von Gruenewaldt et al., 1986; Wilson and Chunnett, 2007) and chromite-poor J-M reef and A and B chromitites of the Stillwater Complex (Page et al., 1985; Barnes and Naldrett, 1986). Mechanisms responsible for concentrating PGE in mafic–ultramafic intrusions may vary from deposit to deposit (Naldrett, 2004). In a most intriguing model for the Merensky Reef of the Bushveld Complex, PGE-rich magma was proposed and this magma was thought to be a result of multistage-dissolution of pre-existing sulfides by sulfide-undersaturated magmas (Kerr and Leitch, 2005; Naldrett et al., 2009). However, evidence for the existence of such PGE-rich magma is still lacking because examples of PGE-dominated deposits formed in this way are sparse.

A number of magmatic sulfide deposits are hosted in small mafic–ultramafic intrusions of the Emeishan Large Igneous Province (ELIP) (Zhou et al., 2002a, 2008). These sulfide deposits have variable Ni, Cu and PGE concentrations and are thought to have formed through concentration of sulfide in staging magma chambers or in dynamic magma conduits (Wang and Zhou, 2006; Tao et al., 2007, 2008; Song et al., 2008). Most of the deposits are Ni–Cu-dominated and sulfide-rich, such as the Baimazhai, Limahe and Yangliuping deposits (Wang and Zhou, 2006; Song et al., 2008; Tao et al., 2008). The only PGE-

* Corresponding author. Tel./fax: +86 20 8529 1803.
E-mail address: wang_yan@gig.ac.cn (C.Y. Wang).

0024-4937/$ – see front matter © 2010 Elsevier B.V. All rights reserved.
doi:10.1016/j.lithos.2010.07.022

dominated and sulfide-poor deposit is the Jinbaoshan deposit, which is the only economically important Pt–Pd deposit in the ELIP (Wang et al., 2005; Tao et al., 2007), containing ~45 tonnes of Pt and Pd with ore grades ranging from 1 to 5 ppm Pt + Pd (Tao et al., 2007). Unlike the PGE-rich deposit elsewhere worldwide, the Jinbaoshan deposit is hosted in a relatively narrow sill mainly composed of wehrlite. Several PGE-rich horizons containing minor amounts of sulfides (<3%) occur near the base and in the centre of the sill. The factors that control the formation of the PGE-rich horizons are a matter of debate. Wang et al. (2005) found that the chromite of the Jinbaoshan sill has high Cr# (51 to 70), variable Mg# (13 to 57) and that olivine has Fo values of ~84 and Ni ranging from 1020 to 2700 ppm. A high MgO/FeO molar ratio (1.47) of the melt composition is consistent with the crystallization of chromite and olivine from a low-Ti and high-Mg tholeiitic magma (Wang et al., 2005). Whereas the Pt and Pd mineralization is closely associated with sulfide, both euhedral chromite enclosed in olivine and olivine itself are usually PGE-barren (Wang et al., 2008), therefore, the PGE-rich horizons were considered to be caused by delayed sulfide saturation by chromite crystallization until the magmas emplaced into an upper magma chamber (Wang et al., 2005). Tao et al. (2007) studied the geochemistry of PGE-rich and PGE-poor wehrlites and envisioned that sulfide saturation occurred at depth in response to olivine and chromite crystallization and that high PGE concentrations of the rocks were achieved when immiscible sulfide droplets accumulated in conduit and reacted with magma successively passing through the conduit. However, such a process is difficult to evaluate without modeling the composition of the rocks.

Platinum-group elements of the mantle-derived rocks are sensitive indicators of the extent of sulfide segregation. Combined with Ni and Cu, these elements are important for understanding the petrogenesis of the mafic–ultramafic rocks (Lightfoot and Keays, 2005; Maier, 2005). In this study, we present a suite of chalcophile element data of rocks from two drill holes that intersect the Jinbaoshan sill, together with major and trace element data. We aim to better understand the sulfide saturation history of the magmas from which the Jinbaoshan sill formed and to develop an integrated model for the formation of the deposit.

2. Geological background

Southwest China is composed of the Yangtze Block to the east and the Tibetan Plateau to the west. The Red River Fault, a left-lateral strike-slip fault, separates the Yangtze Block from the Indochina Block on the southwest. The ELIP occurs chiefly in the western part of the Yangtze Block and extends over much of SW China and northern Vietnam covering an area of more than 0.5×10^6 km^2. The ELIP consists of a sequence of continental flood basalts ranging in thickness from several hundred meters up to 5 km, and spatially associated mafic–ultramafic intrusions. It is believed to have formed by a mantle plume at ~260 Ma (Chung and Jahn, 1995; Xu et al., 2001; Zhou et al.,

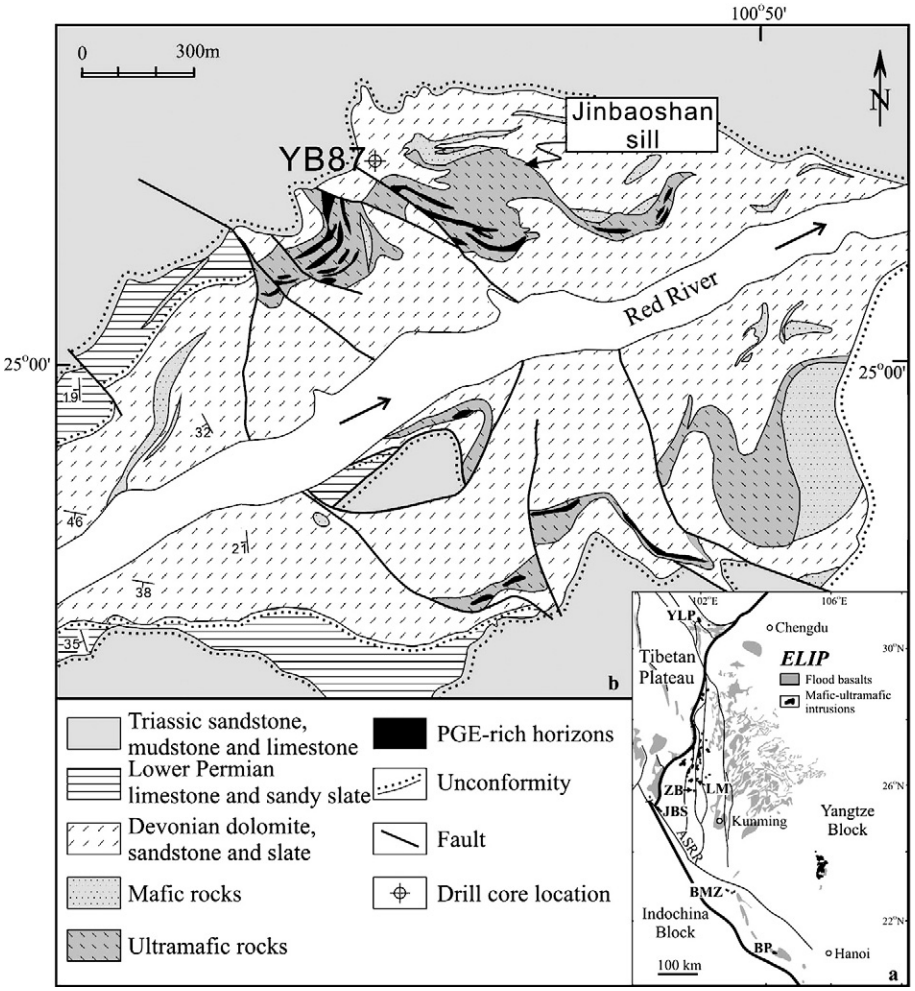

Fig. 1. Geological map and location of the Jinbaoshan area, Yunnan Province, SW China. (a) Regional geology of the Emeishan Large Igneous Province and associated mafic–ultramafic intrusions/sills in SW China and northern Vietnam, YLP—Yangliuping intrusion, LM—Limahe Intrusion, ZB—Zhubu Intrusion, JBS—Jinbaoshan sill, BMZ—Baimazhai Intrusion, BP-Ban Phuc intrusion; (b) Distribution of mafic–ultramafic sills and ore bodies in the Jinbaoshan area (based on an unpublished report of the Geological Team 3, Yunnan Geological Survey).

2002b). Along the western margin of the Yangtze Block, the volcanic succession of the ELIP is strongly deformed, uplifted and eroded following the India–Eurasia collision. Consequently many mafic–ultramafic intrusions are exposed by N–S-trending faults in this region (Fig. 1a). Some of the intrusions host economically important Ni–Cu–(PGE) sulfide deposits including, from north to south, the Yangliuping, Limahe, Zhubu, Jinbaoshan and Baimazhai deposits in SW China and the Ban Phuc deposit in northern Vietnam (Fig. 1a).

In the Jinbaoshan area, there are 21 mafic and 11 ultramafic sills intruding the Devonian and lower Permian strata (Fig. 1b). The ultramafic sills have intrusive relationships with associated mafic sills. The Devonian strata consist of interlayered dolomite, sandstone and slate, whereas the lower Permian strata are limestone and sandy slate. The Devonian and Permian strata form an anticline-like dome, which is separated from Triassic strata by an unconformity and cut by the Red River (Fig. 1b).

The Jinbaoshan sill is about 4760 m long, 760 to 1240 m wide and 8 to 170 m thick, being the largest ultramafic sill in the area. It is dated at 259.2 ± 4.5 Ma using the SHRIMP zircon U–Pb technique (Tao et al., 2009). The sill contains three major PGE-rich horizons, which are defined as rocks having >0.5 ppm Pt + Pd. The boundaries between the PGE-rich horizons and host rocks are transitional. The largest PGE-rich horizon at the base of the sill is about 2100 m long, 400 to 600 m wide and 4 to 16 m thick and accounts for 44% of the total ore reserve (cf. Wang et al., 2005). Two relatively small PGE-rich horizons are located in the middle to upper parts of the sill (Fig. 2a). A chromite-rich layer several tens of centimeter wide occurs discontinuously at the base of the sill, which contains chromite less than 20 vol.% (unpublished report of the Geological Team 3, Yunnan Geological Survey) (see Fig. 1 in Wang et al., 2008).

3. Petrography

Forty-three samples were collected from two drill holes, YB87-1 and YB87-2, which make up a ~110 m composite profile intersecting the Jinbaoshan sill. Sample locations in the profile are shown in Fig. 2b. The section can be divided into six layers based on Pt and Pd concentrations of the rocks, three PGE-rich layers (Layers I, III and V) are interlayered with three PGE-poor layers (Layers II, IV and VI) (Fig. 2b).

The PGE-rich layers have a primary silicate mineral assemblage similar to the PGE-poor layers. The primary rock-forming minerals are olivine and clinopyroxene displaying a granular to poikilitic texture. Olivine occurs as euhedral to subhedral crystals or as rounded grains, with grain sizes increasing from the base and varying from 0.3 to 4 mm. Clinopyroxene occurs as anhedral poikilitic crystals 3 to 8 mm across. Hydrothermal alteration is ubiquitous in the intrusion (Wang et al., 2008). Most olivine grains have been altered to serpentine, and

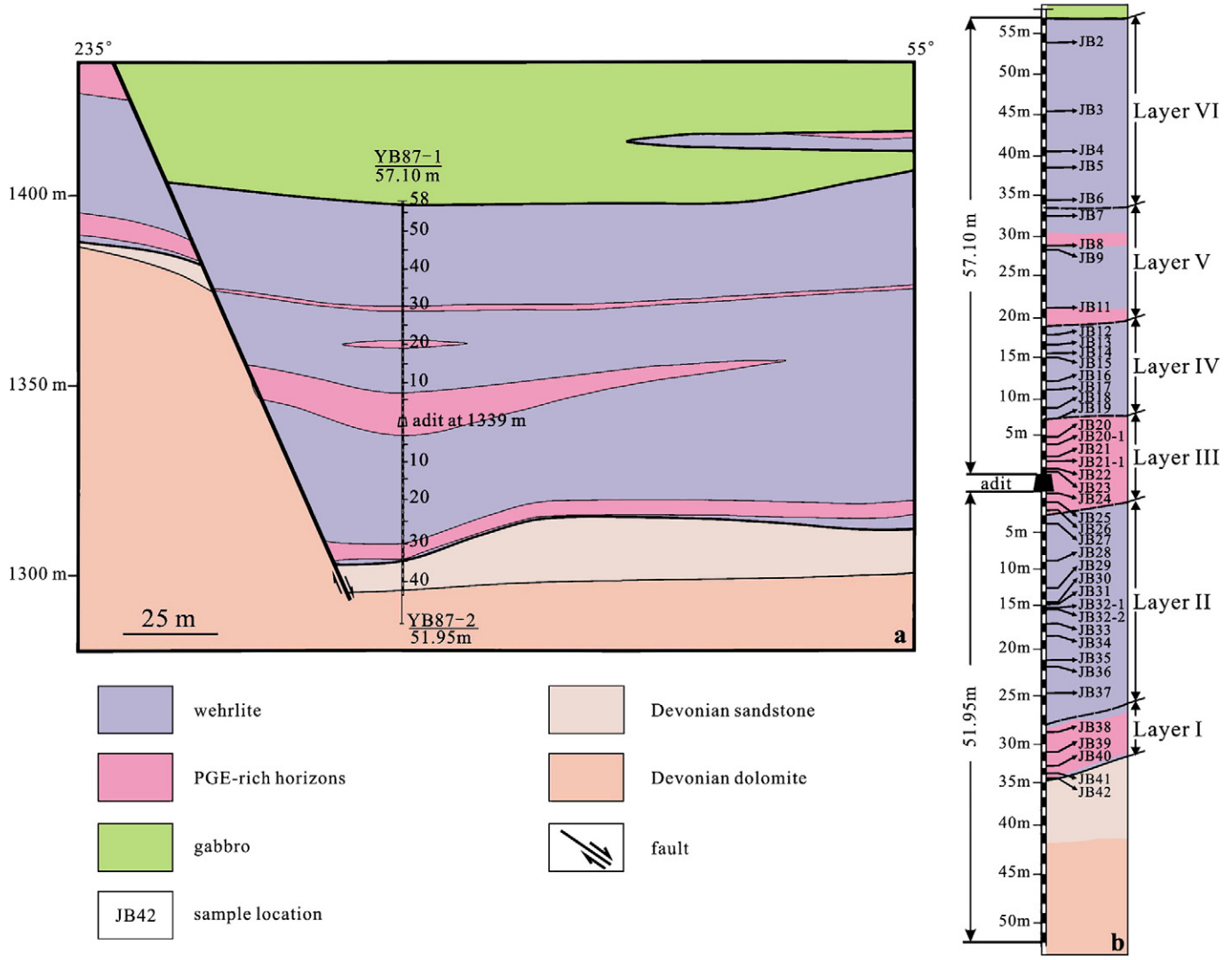

Fig. 2. (a) A cross section of the Jinbaoshan sill along 315 N2 exploration line, showing the distribution of rock units (after the Yunbao platinum and palladium Mining Company, 2004); (b) relative positions of each sample are shown in the columns of drill holes YB87-1 and YB87-2.

interstitial clinopyroxene is often altered to actinolite/tremolite and locally biotite.

Primary chromite occurs either as small euhedral grains (<20 μm) enclosed within olivine, or as zoned interstitial phases altered to magnetite during serpentinization (Wang et al., 2005). No sulfide minerals are visible in hand specimen. However, pyrrhotite, pyrite, pentlandite, chalcopyrite and violarite were observed in thin sections, some of which are closely associated with Te-, Sn- and As-bearing platinum-group minerals (PGM), such as moncheite ($PtTe_2$), atokite (Pd_3Sn), sperrylite ($PtAs_2$), irarsite (IrAsS), cooperite (PtS) and Pt–Fe alloy (Wang et al., 2008). Fine sulfide veinlets along the fractures of silicate minerals indicate late element mobility due to hydrothermal alteration.

The amounts of chromite and sulfide in the Jinbaoshan sill are variable from layer to layer. The rocks usually contain less than 10% chromite and less than 3% sulfide, but some rocks may contain up to 20% chromite or 10% sulfide. Cumulus olivine (now serpentine) grains are surrounded by irregular chromite grains, forming an orbicular texture in the rocks of the chromite-rich layer (Fig. 3a). Such orbicular texture is also occasionally observed at the top of Layer II. Sulfide (<1%) is rarely observed in the chromite-rich layer. PGE-rich Layer I contains abundant sulfide (up to 10%) interstitial to silicate phases (Fig. 3b). Only minor interstitial chromite (<5%) is closely associated with sulfide (Fig. 3c). PGE-rich Layer III also has sulfide and associated chromite interstitial to silicate phases, but contains interstitial chromite (5 to 10%) apparently more abundant than Layer I (Fig. 3d–e). PGE-rich Layer V only has minor interstitial sulfides (<1%) relative to large amount of interstitial chromite (5 to 10%) (Fig. 3f). PGE-poor Layers II, IV and VI have similar textures to Layer V, with the amounts of sulfide and chromite varying slightly from sample to sample.

4. Analytical methods

In this study, PGE were measured by isotope dilution (ID)-ICP-MS after digestion of samples using a modified Carius tube technique (Qi et al., 2007; Qi and Zhou, 2008) at the PGE lab in the Department of Earth Sciences, University of Hong Kong. Twelve grams of rock

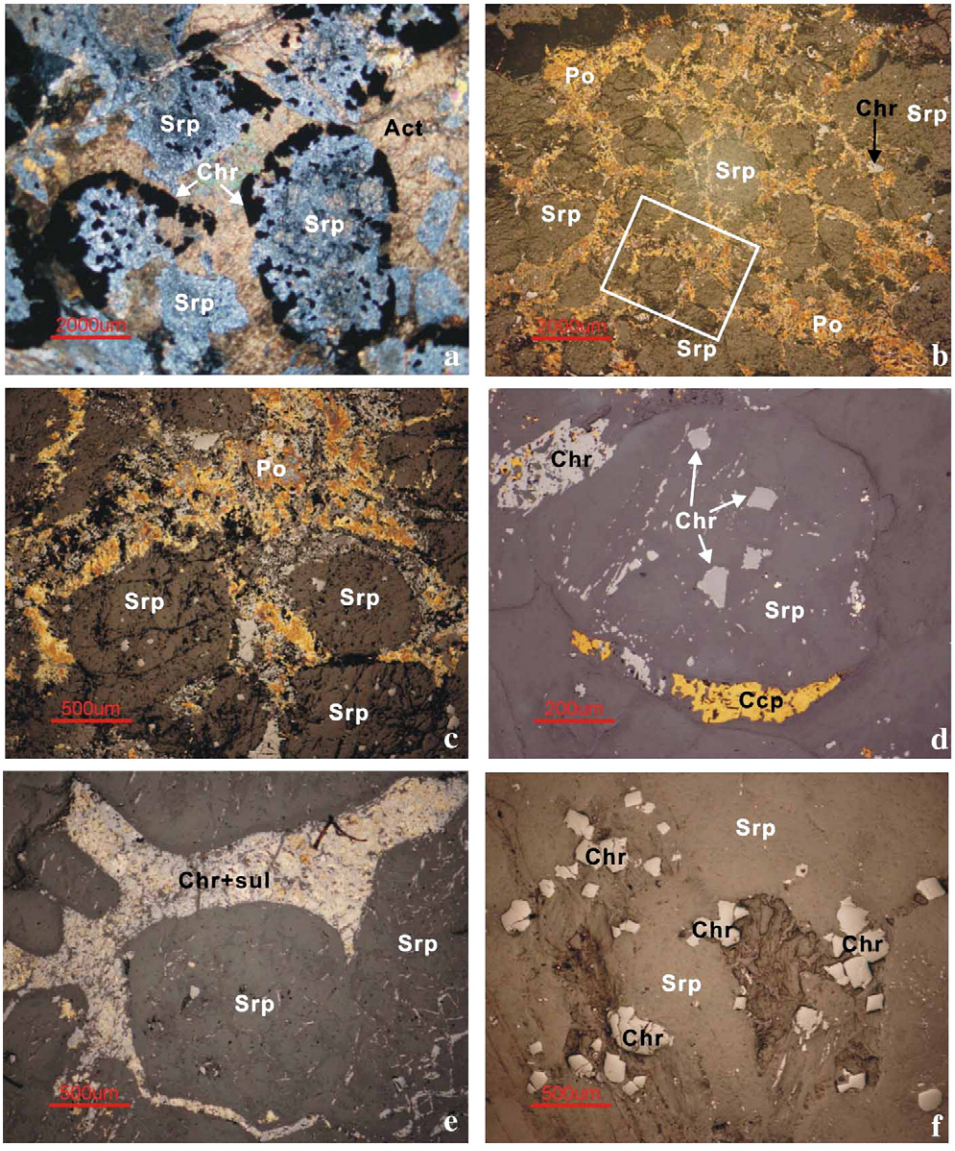

Fig. 3. Photomicrographs of rocks in PGE-rich and PGE-poor layers of the Jinbaoshan sill. (a) Podiform-like texture with irregular chromite (Chr) grains surrounding cumulate olivine (now serpentine, Srp) grains, clinopyroxene (now actinolite, Act) as an interstitial phase. Under cross polarizer, transmitted light; (b) large amount of pyrrhotite (Po) associated with chromite (Chr) are interstitial to cumulate olivine (now Serpentine) grains in sample JB-42 from Layer I, reflected light; (c) close-up of (b) showing intergrowth of pyrrhotite and chromite; (d) intergrowth of chromite and chalcopyrite (Ccp) to olivine (now serpentine) in sample JB-23 from Layer III, reflected light; (e) intergrowth of chromite and sulfide as interstitial phases in sample JB-9 from Layer V, reflected light; (f) chromite interstitial to olivine (now serpentine) in PGE-poor layers, reflected light.

powder and an appropriate amount of enriched isotope spike solution containing ^{193}Ir, ^{101}Ru, ^{194}Pt and ^{105}Pd were digested with 35 ml aqua regia in a 75 ml Carius tube, which was placed in a custom-made high-pressure autoclave filled with water to prevent explosion of the tube when heated. After heating for 10 h at 300 °C, the Carius tube was cooled and the contents were transferred to a 50 ml centrifuge tube. After centrifuging, the residue was discarded and the solution was used to pre-concentrate PGE by Te coprecipitation. The main interfering elements, including Cu, Ni, Zr and Hf were removed by a mixed ion exchange column which contained a Dowex 50 WX 8 cation exchange resin and a P507 extraction chromatograph resin. Platinum, Pd, Ru and Ir were measured by isotope dilution, whilst ^{194}Pt was used as the internal standard to calculate the abundance of the mono-isotope element, Rh (Qi et al., 2004). Measurement was done by a VG Plasma-Quad Excell ICP-MS. Analytical results for standard reference materials, WPR-1 (peridotite) and UMT-1 (ultramafic ore tailings), and WMS (sulfide ore), are in good agreement with the certified and published values (Appendix A). The total procedural blanks were lower than 0.003 ppb for Ru, Rh and Ir, 0.018 ppb for Pt, and 0.037 ppb for Pd. Analytical results are listed in Table 1.

Whole-rock S contents were obtained using IR-absorption spectrometry at the Institute of Geochemistry, Chinese Academy of Sciences. The detection limit of the IR-absorption spectrometry is about 10 μg/g and the accuracies are estimated to be better than ±8%. Results are listed in Table 1.

Major element oxides were determined by wavelength-dispersive X-ray fluorescence spectrometry (WD-XRFS) on fused glass beads using a Rigaku100e spectrometer at the Guangzhou Institute of Geochemistry, Chinese Academy of Sciences. The accuracies of the XRF analyses are estimated to be ±2% (relative) for major oxides present in concentrations greater than 0.5 wt.% and ±5% (relative) for minor oxides greater than 0.1%.

Trace elements were determined by inductively coupled plasma mass spectrometry (ICP-MS) using a VG Plasma-Quad Excell ICP-MS at the Department of Earth Sciences, the University of Hong Kong, after a 2-day closed-beaker digestion using a mixture of HF and HNO_3 acids in high-pressure bombs (Qi et al., 2000). The accuracies of ICP-MS analyses are estimated to be better than ±5% (relative) for most elements. Analytical results of major and trace elements of the rocks are listed in Table 2.

5. Analytical results

5.1. Stratigraphic variations

The concentrations of Cr, Ni, Cu, S and PGE of the rocks are plotted against the stratigraphic heights (Fig. 4). PGE-rich Layer I contains remarkably low Cr but high Ni, Cu and S contents relative to the other layers (Fig. 4a–d). Layers II, III, IV, V and VI have less variable Cr and Ni contents (Fig. 4a–b) but highly variable Cu and S contents (Fig. 4c–d)

Table 1
Sulfur and chalcophile element concentrations of the rocks from the Jinbaoshan sill.

Sample No.	S (wt.%)	Sulfide (wt.%)	Ni (ppm)	Ir (ppb)	Ru (ppb)	Rh (ppb)	Pt (ppb)	Pd (ppb)	Cu (ppm)
JB-2	0.30	0.79	797	7.40	5.04	10.2	191	166	31.2
JB-3	0.05	0.14	708	3.45	2.34	3.86	62.5	30.6	9.46
JB-4	0.01	0.26	678	2.20	2.16	3.08	55.3	32.1	15.3
JB-5	0.09	0.23	684	2.40	2.42	3.70	79.1	36.5	6.36
JB-6	0.08	0.22	679	4.64	2.37	3.69	53.9	21.9	7.98
JB-7	0.10	0.27	734	8.04	4.31	8.25	100	115	20.3
JB-8	0.16	0.41	774	7.46	4.23	8.15	153	139	32.4
JB-9	0.39	1.02	1030	25.1	16.5	38.0	844	673	321
JB-11	0.17	0.45	811	10.8	8.21	15.1	327	322	209
JB-12	0.10	0.25	743	3.26	2.50	4.62	56.3	32.4	16.1
JB-13	0.09	0.24	742	6.96	4.62	10.1	159	152	14.4
JB-14	0.09	0.23	720	5.80	3.29	5.23	62.8	48.5	16.0
JB-15	0.10	0.26	775	9.91	5.10	12.2	177	172	16.1
JB-16	0.09	0.22	590	4.78	2.85	5.14	69.6	34.5	12.5
JB-17	0.10	0.27	847	4.50	4.06	7.51	135	105	16.5
JB-18	0.24	0.63	773	13.2	8.12	17.3	266	361	230
JB-19	0.12	0.31	816	8.13	5.84	12.8	193	218	13.4
JB-20	0.11	0.28	883	16.4	10.6	25.8	486	614	12.3
JB-20-1	0.29	0.76	828	19.8	13.0	35.3	695	829	82.1
JB-21	0.26	0.67	1041	67.2	26.0	79.0	1400	1878	736
JB-21-1	0.27	0.70	1053	54.2	35.9	96.1	1367	2311	555
JB-22	0.20	0.53	1111	47.9	37.5	107	2518	2852	248
JB-23	0.32	0.85	1027	50.1	29.8	94.4	1713	2330	821
JB-24	0.19	0.49	926	46.1	17.6	48.4	880	1455	357
JB-25	0.13	0.35	801	12.1	4.94	14.6	230	363	43.5
JB-26	0.11	0.28	772	2.78	1.39	4.40	41.1	58.7	27.4
JB-27	0.09	0.23	583	2.57	1.14	3.93	44.4	32.8	7.35
JB-28	0.10	0.27	570	3.20	1.37	4.44	50.3	57.5	18.9
JB-29	0.08	0.20	705	4.06	2.17	7.68	109	178	11.4
JB-30	0.10	0.27	746	5.27	3.49	12.7	215	396	31.9
JB-31	0.09	0.24	736	7.19	4.53	8.29	117	149	9.45
JB-32-1	0.15	0.38	717	14.4	4.34	20.3	298	596	249
JB-32-2	0.09	0.24	643	3.66	1.65	5.11	92.9	132	36.5
JB-33	0.10	0.25	708	5.49	2.99	10.2	170	272	47.5
JB-34	0.100	0.27	759	8.18	4.82	17.4	289	505	49.0
JB-35	0.09	0.23	709	5.64	2.76	9.72	125	208	7.72
JB-36	0.24	0.63	677	6.65	3.67	14.7	225	383	350
JB-37	0.08	0.21	544	1.66	0.87	3.45	50.5	105	14.8
JB-38	0.44	1.16	738	15.9	7.15	25.1	439	530	275
JB-39	0.89	2.34	835	47.2	10.13	35.6	564	786	1261
JB-40	4.28	11.26	1926	138	38.7	133	654	3696	508
JB-41	4.31	11.34	1904	55.2	37.3	116	987	1593	2580
JB-42	4.36	11.47	1824	51.6	38.9	121	704	1498	2902

Table 2
Major and trace elements of the rocks from the Jinbaoshan ultramafic sill.

Sample No.	JB-2	JB-4	JB-6	JB-8	JB-11	JB-13	JB-15	JB-17	JB-19	JB-20	JB-22	JB-24	JB-26	JB-28	JB-30	JB-35	JB-39	JB-41
Layers	VI	VI	VI	V	V	IV	IV	IV	IV	III	III	III	II	II	II	II	I	I
depth (m)	107.95	94.45	88.45	82.95	74.95	70.65	68.95	64.95	61.15	58.75	54.75	54.15	49.45	43.15	37.55	30.95	20.95	18.05
Major oxide (wt.%)																		
SiO_2	37.40	36.57	34.14	40.52	37.91	38.35	39.71	38.47	39.35	37.14	40.42	37.25	40.19	35.34	38.18	40.12	37.04	32.50
TiO_2	0.45	0.44	0.43	0.45	0.42	0.42	0.53	0.44	0.51	0.53	0.53	0.46	0.49	0.46	0.53	0.49	0.60	0.46
Al_2O_3	2.67	2.25	2.59	2.95	2.57	2.98	2.58	3.51	3.13	3.06	3.36	2.57	3.06	3.43	2.97	3.08	3.04	2.59
Fe_2O_{3total}	15.14	15.76	12.57	7.31	13.57	12.58	11.39	11.52	10.20	14.52	9.12	14.49	8.64	20.19	14.13	12.70	18.24	19.58
MgO	32.17	33.61	30.40	36.22	34.77	34.88	34.72	35.21	35.24	33.34	35.28	33.76	36.32	29.94	32.07	31.65	28.29	25.95
MnO	0.09	0.17	0.15	0.17	0.13	0.16	0.15	0.15	0.16	0.17	0.18	0.13	0.16	0.18	0.16	0.16	0.16	0.17
CaO	0.27	0.14	5.05	0.54	0.22	0.15	0.40	0.20	0.60	0.62	0.86	0.57	0.22	1.00	1.43	2.74	2.87	3.51
K_2O	0.16	0.10	0.13	0.16	0.14	0.11	0.19	0.10	0.17	0.18	0.16	0.15	0.14	0.15	0.16	0.09	0.05	0.08
Na_2O	0.09	0.01	0.20	0.05	0.05	0.02	0.07	0.02	0.06	0.51	0.07	0.05	0.02	0.45	0.06	0.20	0.07	0.02
P_2O_5	0.05	0.04	0.04	0.04	0.03	0.03	0.05	0.04	0.04	0.06	0.05	0.04	0.04	0.03	0.05	0.03	0.05	0.04
LOI	11.21	10.48	14.76	11.42	10.78	10.90	10.75	10.91	11.19	10.31	10.51	10.94	11.44	9.03	10.76	8.99	9.18	13.12
Total	99.70	99.57	100.45	99.83	100.60	100.59	100.53	100.58	100.66	100.45	100.52	100.41	100.70	100.20	100.50	100.24	99.59	98.02
Trace element (ppm)																		
Sc	9.00	11.1	10.4	7.69	7.70	4.36	8.67	6.30	10.1	6.16	7.26	7.10	5.83	7.13	15.3	16.5	20.7	15.9
V	101	101	103	106	97.5	104	119	121	121	111	118	99.3	123	126	139	152	176	137
Cr	6471	6285	6440	6834	6683	7614	7209	8720	8316	7346	8102	7314	9098	8760	8023	9450	4633	3947
Co	183	207	168	149	206	176	184	191	177	158	165	172	199	157	180	178	212	396
Rb	6.00	3.99	4.53	5.31	3.92	3.67	6.37	3.91	6.44	5.51	5.56	4.84	5.35	3.68	4.20	2.84	3.15	3.06
Sr	8.67	4.52	56.35	8.54	10.09	5.76	8.20	6.16	13.33	9.95	9.36	10.55	8.21	8.25	20.30	18.16	18.19	48.43
Y	3.67	2.74	3.52	4.29	3.18	2.99	3.66	3.80	4.52	4.31	4.67	3.77	4.35	3.67	4.02	3.98	5.45	5.07
Zr	26.7	28.2	25.2	29.0	27.9	22.7	36.6	22.2	34.5	34.3	36.6	30.6	34.5	22.0	32.3	18.0	35.6	22.1
Nb	3.20	3.32	2.94	3.22	3.16	2.64	4.00	2.57	3.71	3.81	3.78	3.39	4.08	2.38	3.51	1.81	2.97	2.82
Cs	3.13	0.92	2.11	1.95	1.00	1.18	1.48	1.52	2.04	1.32	1.43	1.02	1.10	1.36	1.43	1.51	1.88	1.59
Ba	37.0	26.3	31.3	36.0	30.7	23.8	40.2	22.0	43.0	33.8	30.7	27.8	27.1	27.1	33.4	34.3	20.0	18.7
La	5.70	3.34	4.59	4.43	3.31	3.18	4.17	3.37	4.78	5.36	5.01	4.43	5.40	3.13	4.47	3.86	3.67	3.15
Ce	12.18	7.50	10.07	9.62	7.28	7.12	9.62	8.32	10.29	12.72	11.08	9.02	12.47	7.80	9.47	8.62	9.03	7.01
Pr	1.45	0.87	1.31	1.29	0.91	0.88	1.22	1.12	1.30	1.57	1.41	1.11	1.56	1.04	1.20	1.10	1.30	0.95
Nd	5.81	3.54	5.00	5.29	3.44	3.28	4.45	4.28	4.94	5.88	5.67	4.41	5.86	4.30	4.54	4.58	5.13	4.15
Sm	1.11	0.72	1.09	1.23	0.84	0.72	1.09	1.00	1.13	1.16	1.35	1.01	1.43	1.12	1.01	1.13	1.39	1.11
Eu	0.20	0.17	0.41	0.34	0.15	0.18	0.26	0.18	0.39	0.35	0.32	0.26	0.30	0.24	0.23	0.38	0.38	0.26
Gd	1.47	1.05	1.15	1.50	1.32	1.19	1.48	1.22	1.39	1.38	1.57	1.17	1.43	1.15	1.22	1.21	1.40	1.27
Tb	0.15	0.11	0.15	0.20	0.13	0.11	0.17	0.14	0.18	0.18	0.19	0.15	0.18	0.17	0.17	0.16	0.21	0.17
Dy	0.82	0.59	0.75	0.98	0.64	0.66	0.81	0.79	0.92	0.95	1.02	0.81	0.93	0.82	0.82	0.88	1.13	0.99
Ho	0.18	0.13	0.15	0.20	0.13	0.13	0.17	0.16	0.19	0.20	0.21	0.16	0.19	0.15	0.18	0.18	0.24	0.22
Er	0.44	0.31	0.42	0.51	0.35	0.35	0.46	0.44	0.53	0.49	0.52	0.45	0.49	0.41	0.48	0.48	0.59	0.57
Tm	0.06	0.04	0.05	0.07	0.05	0.05	0.06	0.07	0.08	0.06	0.08	0.06	0.07	0.06	0.06	0.07	0.08	0.07
Yb	0.33	0.28	0.32	0.42	0.33	0.32	0.39	0.40	0.49	0.42	0.47	0.41	0.42	0.34	0.39	0.43	0.56	0.46
Lu	0.06	0.04	0.05	0.07	0.05	0.05	0.07	0.07	0.07	0.07	0.08	0.06	0.07	0.06	0.07	0.06	0.09	0.07
Hf	0.77	0.76	0.75	0.76	0.74	0.63	0.92	0.62	0.93	0.91	0.98	0.83	0.95	0.62	0.92	0.75	1.02	0.61
Ta	0.24	0.24	0.22	0.23	0.21	0.19	0.28	0.17	0.29	0.27	0.27	0.23	0.28	0.16	0.27	0.15	0.22	0.18
Th	0.75	0.82	0.67	0.70	0.66	0.57	0.92	0.64	0.89	0.89	0.87	0.79	0.84	0.59	0.85	0.43	0.60	0.59
U	0.17	0.45	0.27	0.15	0.49	0.18	0.21	0.16	0.19	0.19	0.19	0.16	0.19	0.15	0.18	0.09	0.19	0.16

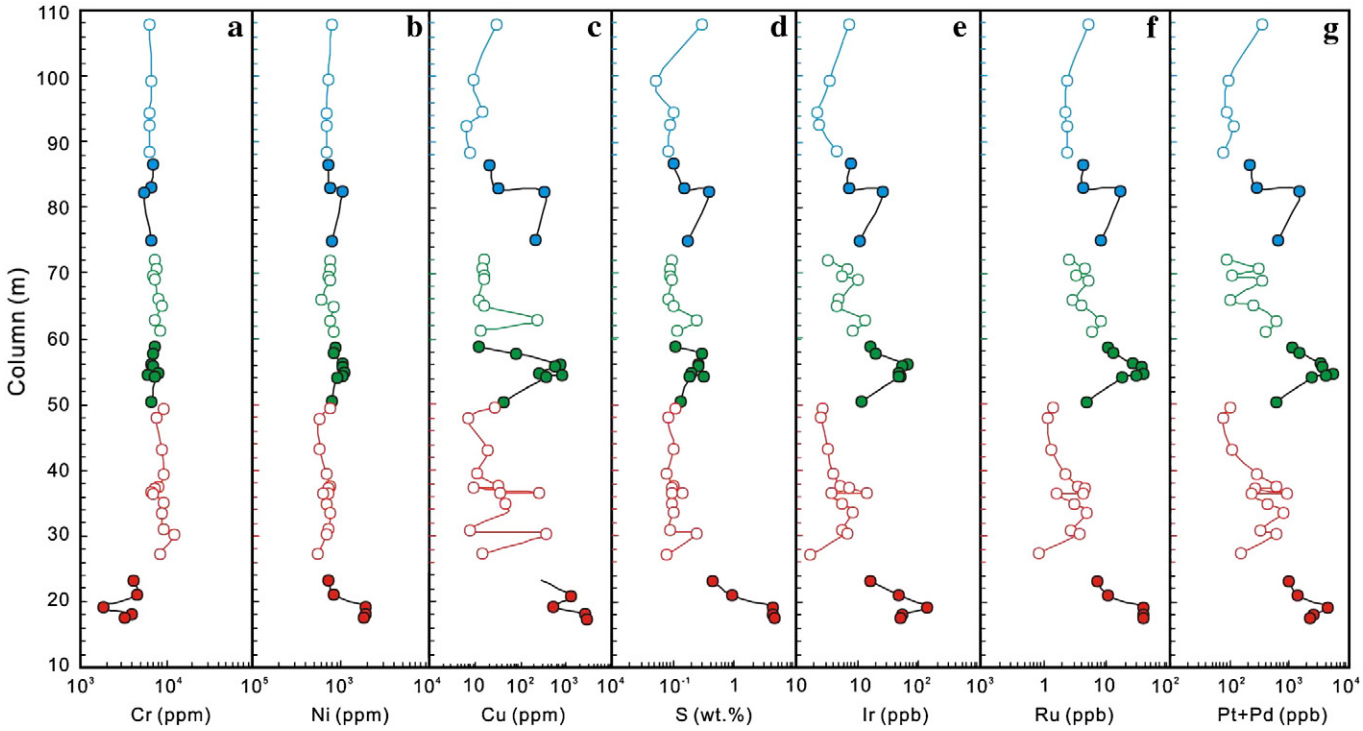

Fig. 4. Variations in Cr, Ni, Cu, S, Ir, Ru and Pt + Pd with relative stratigraphic position. Assigned relative stratigraphic positions together with the depth or elevation of the original sample are given in Fig. 2b.

relative to Layer I. However, S and Cu contents of Layers II to VI are generally low (<0.4 wt.%S, and <1000 ppm Cu), consistent with the scarcity of visible sulfides in the rocks. As a result the PGE-rich layers cannot be distinguished macroscopically. Amongst the PGE-rich layers, Layers I and III have distinctly higher PGE concentrations than Layer V (Fig. 4e–g).

5.2. Compositional variation between PGE-rich and PGE-poor layers

PGE, Cu and Ni concentrations are highly variable from layer to layer. Three samples from Layer I have distinctly high Ni concentrations, whereas other samples show a positive relationship between Ir and Ni (Fig. 5a). Iridium shows a weak positive correlation with Cu (Fig. 5b), but a good positive correlation with Ru, Pt and Pd (Fig. 5c–e). Platinum varies positively with Pd (Fig. 5f). Pd/Ir ratios vary from 14 to 60 in PGE-rich layers and from 5 to 75 in PGE-poor layers (Fig. 5e). Pd/Pt ratios range from 0.4 to 2.1 in PGE-poor layers, whereas they vary from 0.8 to 2.1 with one high exception of 5.7 in PGE-rich layers (Fig. 5f).

Both the PGE-rich layers and PGE-poor layers show identical primitive mantle-normalized chalcophile element patterns (Fig. 6). All the rocks display relatively steep and arched patterns with strong negative Ru anomalies. Both Cu and Ni are very depleted relative to Ir, Rh, Pt and Pd (Fig. 6).

The rocks of PGE-rich Layer I contain high S-rich samples (S = 0.4 to 4.4 wt.%) with three of them having S > 4 wt.%. The sulfide contents calculated based on S of the rocks of Layer I vary from 1.2 to 11.5 wt.%. All the other samples are less S-rich (S = 0.1 to 0.4 wt.%), with low sulfide contents ranging from 0.14 to 1.0 wt.%. In the plot of S versus Ni, Cu and PGE metals, two trends are displayed; one for the rocks from Layer I with lower metal/S ratios, the other for most of the other rocks with higher metal/S ratios (Fig. 7).

The PGE-rich layers generally have Cr contents lower than PGE-poor layers. Bivariant plots of Ir and Pt + Pd versus Cr basically show weak correlation (Fig. 8a and b). PGE-rich layers have sulfide contents varying negatively with Cr, whereas the PGE-poor layers show variable Cr contents at a relatively small range of sulfide contents of the rocks (Fig. 8c).

Cu/Pd ratios of all the rocks are significantly lower than the primitive mantle value of 7000 (Barnes and Maier, 1999). PGE-rich layers have Cu/Pd ratios ranging from 20 to 1938 with an average value of 524 ± 581 ($1\sigma_{n=17}$), whereas PGE-poor layers have Cu/Pd ratios from 37 to 913 with an average of 270 ± 209 ($1\sigma_{n=26}$). PGE-rich layers have Cu/Pd ratios more variable than the PGE-poor layers, with both the highest and lowest Cu/Pd ratios of the rocks from PGE-rich layers (Fig. 9a). Cu/Zr ratios of all the rocks are variable from 0.24 to 134. Most rocks of PGE-rich layers have Cu/Zr ratios >1 with a range from 0.36 to 134; whereas most rocks of PGE-poor layers have Cu/Zr ratios <1 with a range from 0.24 to 13 (Fig. 9b).

6. Discussion

6.1. Effect of hydrothermal alteration

The Jinbaoshan sill has undergone serpentinization and hydrothermal alteration. Wang et al. (2008) considered that hydrothermal fluids were responsible for the release of PGE from sulfides to precipitate PGMs at low temperature. However, a few lines of evidence support a magmatic origin of PGE concentrations of the rocks. Good correlations of Pt and Pd with Ir (Fig. 5d–e) indicate that originally PGE were concentrated by magmatic processes. In general, palladium is preferentially mobilized relative to other PGE by hydrothermal alteration, leading to the flattening from Pt to Pd in the primitive mantle-normalized PGE patterns (Barnes et al., 1985). Most of the samples at Jinbaoshan display steep slopes from Pt to Pd except for a few samples in Layer VI showing slightly flattening from Pt to Pd (Fig. 6f). Moreover, Pd/Pt ratios of most rocks vary in a small range from 1 to 2 (Fig. 5f), together with a positive correlation of Pt and Pd (Fig. 5f), indicating the coherent behavior of these elements during the magma evolution to form the Jinbaoshan sill and generally immobile nature of Pd during hydrothermal alteration.

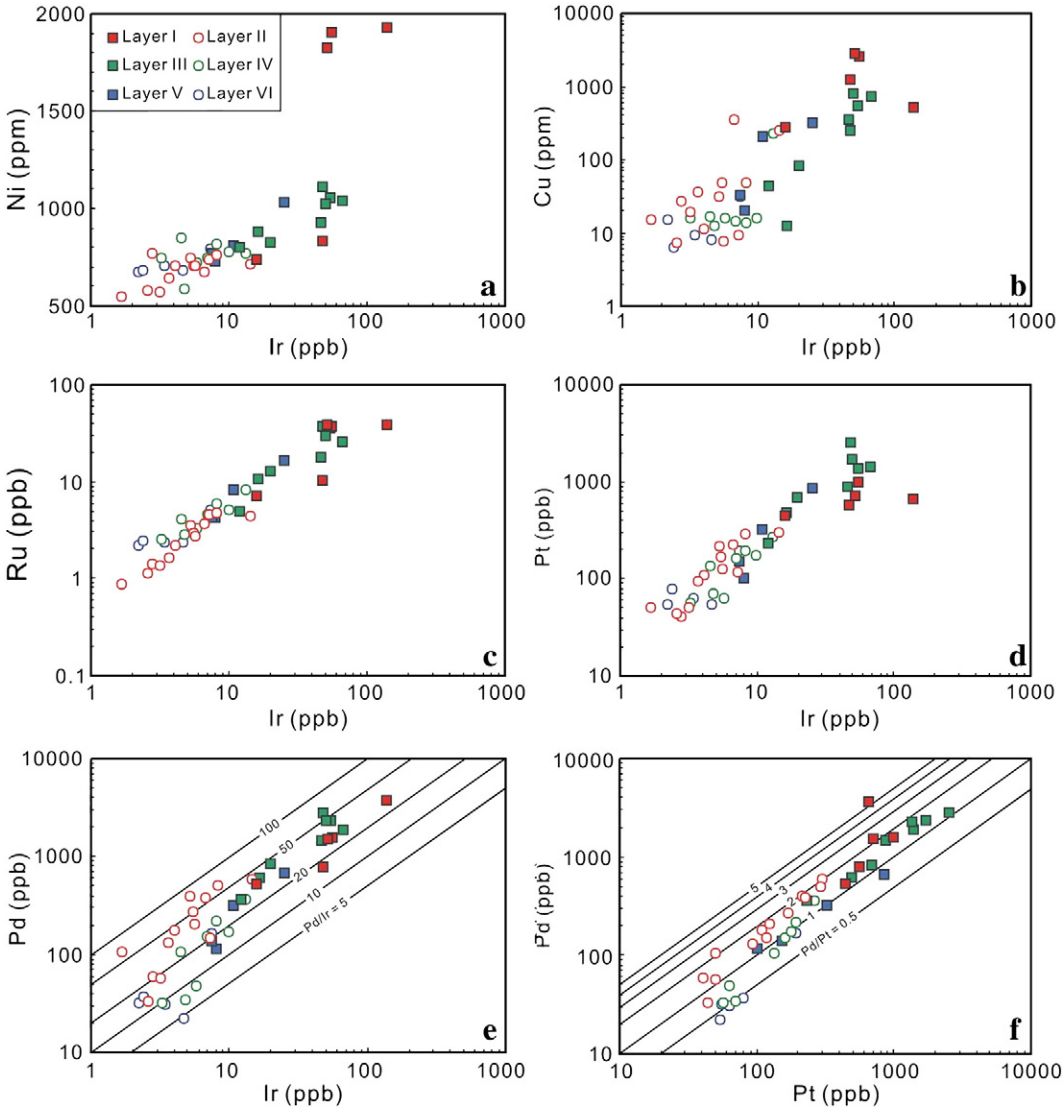

Fig. 5. Plots of Ir versus Ni, Cu, Ru, Pt and Pd, and Pt versus Pd for the rocks from PGE-rich and PGE-poor layers of the Jinbaoshan sill.

The rocks of the PGE-rich layers have high Ir concentrations ranging from 7.5 to 138 ppb (Table 1) and low Pd/Ir ratios (14 to 60) (Fig. 5e). Usually hydrothermal sulfide ores have extremely low Ir, resulting in very high Pd/Ir ratios (Keays et al., 1982), because Pd and Ir are fractionated during alteration (Barnes et al., 1985). Iridium is not easily leached from the source rocks or readily transported by fluids (Keays et al., 1982). The good positive correlation between Ir and Pd of the rocks of the PGE-rich layers (Fig. 5e) indicates a magmatic feature of Ir and Pd. Therefore, the sulfides and PGE of the Jinbaoshan sill were originally concentrated by magmatic processes although the sill has undergone post-magmatic hydrothermal alteration.

6.2. Early crystallization of olivine and chromite from primitive magmas

The measured S content in basaltic melts saturated with sulfide liquids is 0.14 ± 0.02 wt.% (Jugo et al., 2005). Most of the rocks at Jinbaoshan contain >0.1 wt.%S, indicating that a sulfide liquid was present throughout the sill. However, some evidence indicates that early-stage olivine and chromite may have crystallized from primitive magmas before sulfide fractionation.

Previous studies indicated that the olivine of the Jinbaoshan sill has relatively low Ni at a restricted low Fo content of ~84 mol% (<2000 ppm, after Wang et al., 2005; Tao et al., 2007) compared to olivine with similar Fo from the Emeishan picrites (~2500 ppm, after Xu et al., 2001; Fo = 91, Zhang et al., 2006), indicating that the magma from which the olivine crystallized was fairly evolved. The trend with high Ni/S ratios in Fig. 7a yields a sulfide liquid with about 12 wt.% Ni that was present in PGE-poor rocks, whereas the trend with low Ni/S ratio indicates a sulfide liquid with ~2 wt.% Ni was presented in PGE-rich rocks. Given the low sulfide contents of the rocks, Ni in sulfide liquid was quite low, indicating that Ni may likely be controlled by both sulfide liquid and olivine. The plot of Ni versus S indicates that there is ~600 to 800 ppm Ni hosted in olivine (Fig. 7a). Therefore, the primitive magma may have experienced an early-stage crystallization of olivine before sulfide fractionation at depth.

The rocks of the Jinbaoshan sill show strong fractionation of PPGE from IPGE, with pronounced negative Ru anomalies (Fig. 6). Removal of sulfide melts from magmas cannot explain such fractionation and negative Ru anomalies as experiments have confirmed that there is only a slight difference in partition coefficients of individual PGE between sulfide and silicate melts (Bezmen et al., 1994; Peach et al., 1994; Fleet et al., 1996). The rocks of the Jinbaoshan sill display a poor correlation between Cr and Ir and Ru, and Layer I with the highest Ir and Ru contains the lowest Cr (Fig. 8a–b). Chromite of the Jinbaoshan sill therefore is not responsible for the fractionation of IPGE relative to

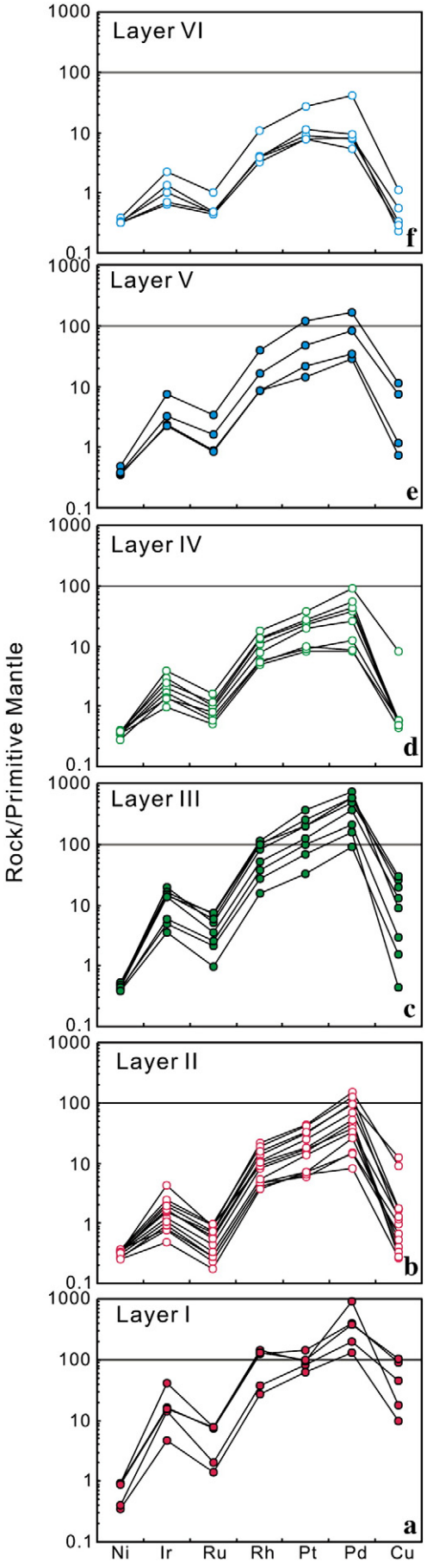

PPGE of the magmas. However, a number of studies have suggested that IPGE may be incorporated in early crystallizing laurite and Os–Ir–Ru alloys (Capobianco and Drake, 1990; Peck and Keays, 1990), which in turn may be physically included as submicroscopic grains in early fractionating phases of chromite and olivine (Stockman and Hlava, 1984; Zhou, 1994; Tredoux et al., 1995; Barnes and Fiorentini, 2008). The chromite grains at Jinbaoshan have Cr# between 51 and 70 (Wang et al., 2005), slightly lower than that of chromite from other mafic–ultramafic intrusions such as Jinchuan (45 to 80, Barnes and Tang, 1999), indicating that there was likely an early-stage of chromite crystallization at depth. In addition, most of PGM grains that have been found at Jinbaoshan are Pt and Pd-dominated, only a few of grains were found to be irarsite (IrAsS) and no Ru-bearing PGM has been found so far (Wang et al., 2008). This may indicate that likely there were laurite (RuS_2) and/or IPGE-bearing alloys trapped in the early crystallizing chromite phases at a depth before the magma was emplaced to form the Jinbaoshan sill, and were responsible for negative Ru anomalies and fractionation of IPGE from PPGE of the rocks.

It is interesting to note that S-poor samples at Jinbaoshan show a good correlation of Ir and Ru versus S (Fig. 7c–d), which is rare in most ultramafic rocks elsewhere and indicates a sulfide control on Ir and Ru. This may indicate that the magma that was depleted in IPGE in the earlier stage was equilibrated with S-undersaturated PGE-undepleted mafic magmas in later stages to gain more Ir and Ru although this process was not able to diminish the depletion of Ru in magmas due to early-stage chromite crystallization.

6.3. Relationship of chromite and sulfide

At Jinbaoshan the chromite-rich layer at the bottom is overlain by the sulfide-rich Layer I. In the chromite-rich layer, rocks contain rare sulfide and show an orbicular texture of several chromite grains surrounding a large olivine grain (Fig. 3a). In other places, closely associated chromite and sulfide are interstitial to olivine and clinopyroxene (Fig. 3c–e). These texture relationships may indicate that chromite and sulfide crystallized after olivine. Then the question is if there was a genetic relationship between chromite and sulfide. It has been documented that the crystallization of chromite can be an important factor controlling the formation of magmatic PGE deposits (Teigler and Eales, 1993; Kinnaird et al., 2002; Kruger et al., 2002) in that the precipitation of chormite would decrease FeO of melts and thus induce sulfide saturation of silicate melts (e.g., Irvine, 1977; Naldrett and von Gruenewaldt, 1989). Given the low sulfide contents of the rocks (generally less than 3%), it can be assumed that large amounts of chromite crystallization from magmas may have played a role for sulfide saturation at Jinbaoshan, given that crustal contamination has been ruled out as a major trigger for sulfide saturation (Tao et al., 2007).

Pd/Cr and Pt/Y ratios are used to examine the relationship of chromite crystallization and sulfide segregation. Chromium is highly compatible in chromite, Pt, Pd and Y are highly incompatible in chromite (Peck and Keays, 1990; Barnes and Fiorentini, 2008). Fractional crystallization of chromite under S-undersaturated condition would result in higher Pd/Cr ratios and nearly constant Pt/Y ratios of the fractionated magmas. In contrast, immiscible sulfide segregation would dramatically decrease Pd/Cr and Pt/Y ratios of the fractionated magmas. On the plot of Pd/Cr versus Pt/Y ratios (Fig. 8d), three samples in the lowest part of Layer I display a trend of increasing Pd/Cr with relatively constant Pt/Y ratios, indicating a fractional crystallization of chromite from S-undersaturated magmas. Pd/Cr and Pt/Y ratios of the other rocks are positively correlated and dramatically decrease from PGE-rich layers to PGE-poor layers. The

Fig. 6. Primitive mantle-normalized chalcophile element patterns for the rocks of PGE-rich and PGE-poor layers of the Jinbaoshan sill. Normalization values of the primitive mantle are from Barnes and Maier (1999) and references therein.

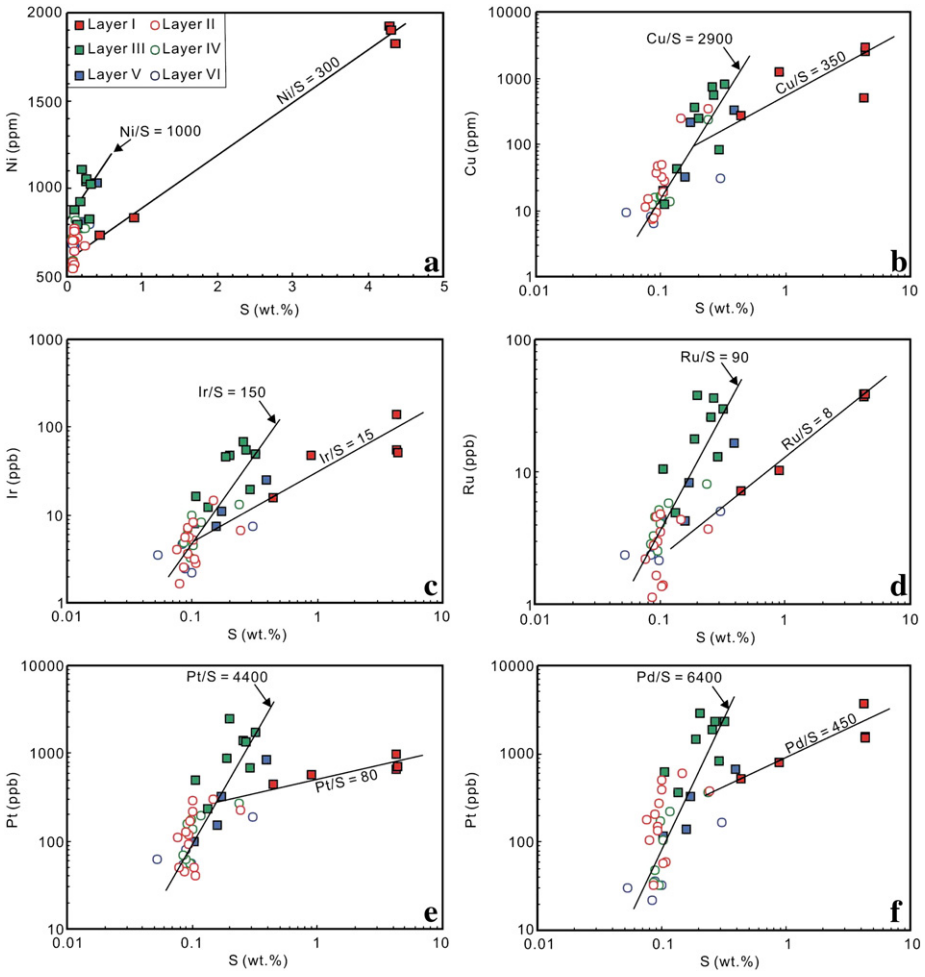

Fig. 7. Plots of S versus Ni, Cu, Ir, Ru, Pt and Pd for the rocks of PGE-rich and PGE-poor layers of the Jinbaoshan sill.

low Pd/Cr and Pt/Y ratios of PGE-poor layers indicate that sulfide liquid with high Pt and Pd was moved from PGE-poor layers to PGE-rich layers with much higher Pd/Cr and Pt/Y ratios (Fig. 8d).

Large amounts of chromite accumulated in chromite-rich layer at Jinbaoshan may be related to an increase of pressure by the replenishment of magma into a magma chamber. Phase relationship indicates that the increase of pressure can shift the fields of crystallization of magma from a phase boundary between orthopyroxene and chromite into the field of chromite which would give rise to the crystallization of chromite only (i.e., a chromite cumulate or chromitite) (Cawthorn, 2005). Large amounts of chromite crystallization may trigger sulfide saturation of the magma. Because chromite (density = 4.5 to 5.09 with an average of 4.79) has a higher density than sulfide minerals (pyhrrotite = 4.6, pantlandite = 4.8, and chalcopyrite = 4.2), dense chromite would settle down quicker than sulfide towards the bottom of the magma chamber, which explains why a chromite-rich sulfide-poor layer is overlain by sulfide-rich Layer I.

6.4. Silicate/sulfide mass ratios (R-factor)

One remarkable feature of the Jinbaoshan sill is very high PGE metal concentrations of the rocks. When calculated to 100% sulfide, the rocks of Layer I with low Ir/S ratios formed when a sulfide liquid with ~1 ppm Ir was present in magmas, whereas the other rocks with relatively high Ir/S ratios formed when a sulfide liquid with ~3 ppm Ir was present. Likewise, it is estimated to have a sulfide liquid with ~30 ppm Pd present in the magmas from which PGE-rich Layer I formed, whereas a sulfide liquid with ~130 ppm Pd was present in magmas for other rocks. Such high PGE in a sulfide liquid would require sulfide segregation from huge amounts of S-undersaturated silicate magmas. The silicate melt/sulfide melt mass ratios (*R*-factor) can be modeled using the equilibrium fractionation equation proposed by Campell and Naldrett (1979):

$$\frac{C_{sulfide}}{C_0} = D \times \frac{(R+1)}{(R+D)}$$

in which $C_{sulfide}$ = the concentration of a trace element in the sulfide liquid, C_o = the initial concentration of that trace element in the silicate liquid, D = the distribution coefficient for the partitioning of the trace element between the sulfide and silicate liquids, and R is the mass ratio of silicate melt to sulfide melt. Assuming a normal primitive magma contains 20 ppb Pd and 90 ppm Cu, the model lines that show the combination of silicate magma with sulfide liquid at different *R*-factors are shown in the plot of Pd versus Cu/Pd proposed by Barnes et al. (1993) (Fig. 10). Three samples of Layer I with the highest sulfide contents (>10 wt.%) and Pd (>400 ppb) can be modeled as a mixture of silicate melt with ~10% sulfide melt at *R*-factor = 1000. Most samples from Layers III and V were modeled as a mixture of silicate melts and 0.1% sulfide at much higher *R*-factors of 10,000 and 100,000. This indicates that the origin of PGE-rich rocks at the Jinbaoshan demands interaction between a large mass of magma and a relatively small mass of sulfide liquid. However, the relationship of coexisting sulfide and silicate liquid in the equation is based on a closed system, in practice very large *R*-factors are difficult to achieve, because finite magmatic diffusion rates and the natural tendency of

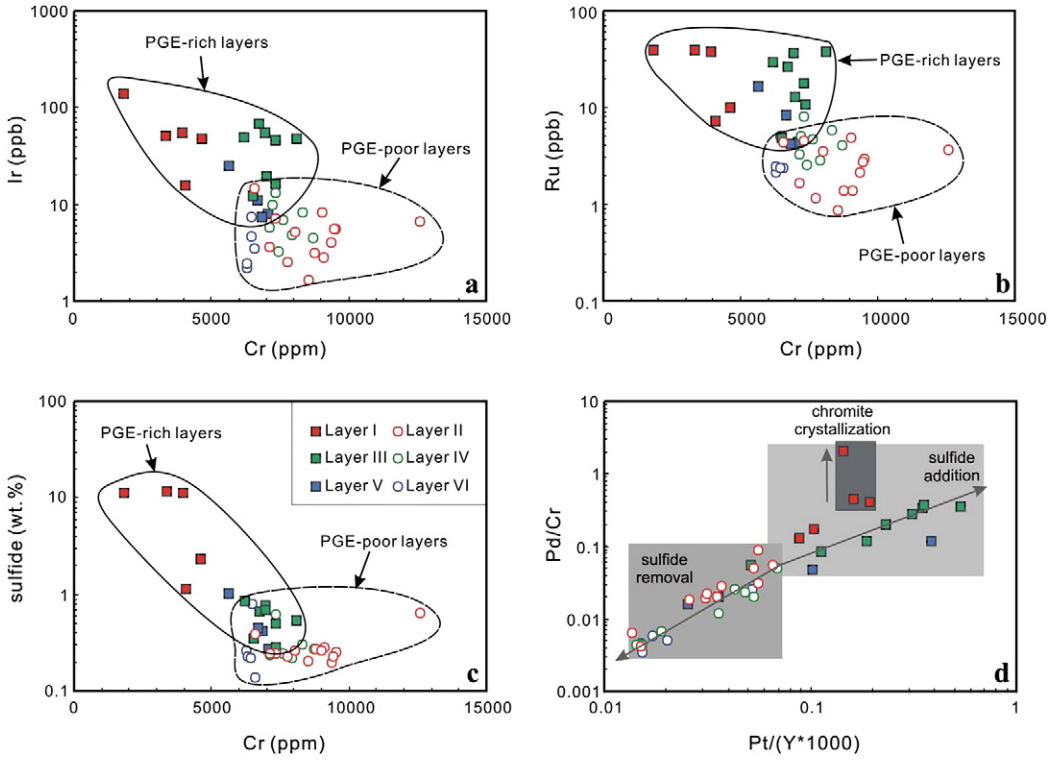

Fig. 8. Plots of Cr versus Ir, Pt + Pd and sulfide content, and Pt/Y versus Pd/Cr for the rocks of PGE-rich and PGE-poor layers of the Jinbaoshan sill.

two immiscible liquids with a remarkably different density to separate from each other would limit the effect of a large *R*-factor (Campell and Naldrett, 1979; Lesher and Campbell, 1993; Mungall, 2002; Kerr and Leitch, 2005). Many workers considered that large *R*-factors could be achieved by a multistage upgrading process in an open system of magma conduit and lava-channel environment, where sulfides readily interact with multiple pulses of magmas, examples including the giant Noril'sk Ni–Cu–PGE deposits (Naldrett et al., 1995, 1996; Naldrett and Lightfoot, 1999), Voisey's Bay (Li and Naldrett, 1999; Naldrett et al., 2000), Uitkomst (Li et al., 2002), and many base metal dominated magmatic sulfide deposits (Lesher, 1989; Lightfoot and Hawkesworth, 1997; Barnes et al., 1999; Naldrett, 1999; Li et al., 2001).

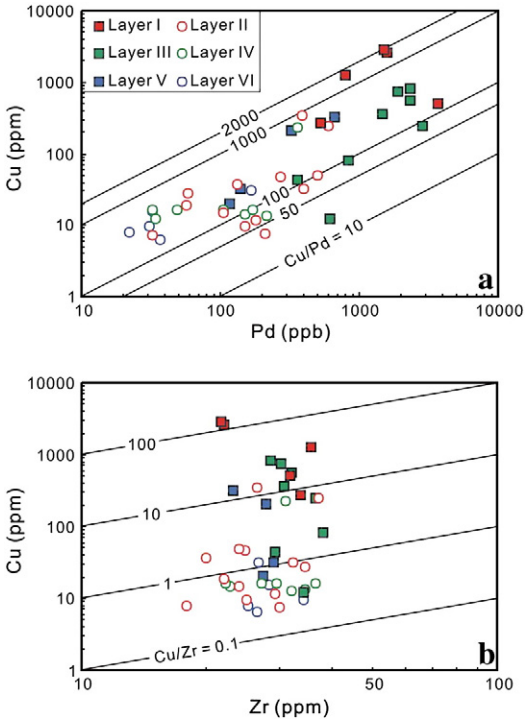

Fig. 9. Variation diagrams of (a) Pd versus Cu, and (b) Zr versus Cu for the rocks of PGE-rich and PGE-poor layers of the Jinbaoshan sill.

6.5. Low Cu/Pd ratios of the rocks

Another interesting feature of the Jinbaoshan sill is that all the rocks have very low Cu/Pd ratios (20 to 2000, Fig. 9a). Usually magma that experienced the removal of sulfide would be highly depleted in

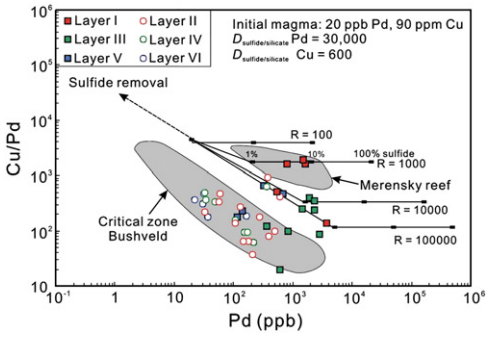

Fig. 10. Plot of Pd versus Cu/Pd for the rocks of PGE-rich and PGE-poor layers of the Jinbaoshan sill showing modeled sulfide composition. Solid lines link the equilibrating silicate liquid and sulfide liquid for various *R*-factors. Divisions on the solid lines indicate 1, 10 and 100% sulfide liquid in the rocks. Shadow fields for Merensky Reef and Critical Zone of the Bushveld Complex are confined with the data from Maier and Barnes (1999).

Table 3
Results of modeling a multistage-dissolution upgrading process for PGE-rich sulfides of the Jinbaoshan sill.

Observed composition at 100% sulfide, Ni corrected for silicates							
Mean value of PGE-rich layers		Ni[a] (wt.%)		Cu (wt.%)		Pt (ppm)	Pd (ppm)
		8.4		3.9		112	147
Parental magma composition[b]		Ni (ppm)		Cu (ppm)		Pt (ppb)	Pd (ppb)
		146		60		11.7	9.99
Modeling results: $R'_{inc}=100$, $L=0.02$							
N	R_{cum}	$f_{sulfide}$	Ni (wt.%) (D=500)	Cu (wt.%) (D=600)	Pt (ppm) (D=10,000)	Pd (ppm) (D=6000)	Pd (ppm) (D=40,000)
21	2642	0.65	7.9	3.9	27.5	21.8	25.6
24	3120	0.62	8.0	3.9	31.9	25.0	30.1
60	11,804	0.30	8.1	4.1	96.8	66.5	107.6
61	12,147	0.29	8.1	4.1	99.0	67.7	110.5
63	12,854	0.28	8.1	4.1	103.4	70.2	116.5
65	13,590	0.27	8.1	4.1	107.9	72.6	122.8
67	14,356	0.26	8.1	4.1	112.4	75.1	129.2
69	15,154	0.25	8.1	4.1	117.1	77.6	135.9
70	15,566	0.24	8.1	4.1	119.4	78.9	139.4
72	16,414	0.23	8.1	4.1	124.2	81.4	146.4

[a] A bulk silicate Ni content of 350 ppm is assumed for correction, using the method of Kerr (2001).
[b] Ni and Cu contents are referred to tholeiite composition for Merensky Reef (after Kerr and Leitch, 2005), and Pt and Pd contents are referred to the ELIP picrites in the northern Vietnam (After Wang et al., 2007).

PGE due to high $D^{sulfide}_{silicate}$ (10^3 to 10^6) of PGE (Bezmen et al., 1994; Fleet et al., 1996), resulting in extremely a high Cu/Pd ratio of residual magma. The low Cu/Pd ratios for the rocks at Jinbaoshan are due to their fairly high Pd concentrations (Table 1), it is thus unlikely that the magmas from which the Jinbaoshan sill formed experienced sulfide removal. Further, the low Cu/Pd ratios of some of the rocks are difficult to reconcile with their Cu/Zr ratios (<1). If the low Cu/Pd ratios of the rocks indicate no sulfide removal from magmas, the rocks that formed from the magmas should have >1 Cu/Zr ratios, rather than <1 Cu/Zr ratios. In general, Cu and Zr are both highly incompatible in sulfide-undersaturated mafic magmas, however, Cu is highly chalcophile whereas Zr is a highly lithophile element that does not partition into sulfide. Therefore, lavas associated with Ni–Cu ore deposits usually have Cu/Zr ratios less than unity (Lightfoot and Keays, 2005). The manner in which the magma acquired high PGE and low Cu/Pd ratios is thus fundamental to the understanding of the upgrading process of the magma.

Most rocks of the PGE-poor layers at Jinbaoshan have low Cu/Pd so that they are distinctly displaced to the left from the modeling lines (Fig. 10), which cannot be readily modeled by a simple silicate–sulfide mixture. The low Cu/Pd ratios of the rocks are similar to those for the Critical Zone of the Bushveld Complex (Maier and Barnes, 1999; Naldrett et al., 2009) (Fig. 10). The origin of the PGE reefs in Bushveld is still under debate. Naldrett et al. (2009) divided available models into two schools, “Uppers” and “Downers”, and evaluated individual models of the two schools. They further interpreted the low Cu/Pd ratios of Pre-Merensky and Merensky cyclic units in the Critical Zone as a result of a derivation of PGE-rich magmas (Naldrett et al., 2009). Earlier than this, Kerr and Leitch (2005) introduced an open-system multistage-dissolution upgrading process to interpret the formation of high PGE concentrations of Ni–Cu–PGE deposits of Noril'sk in Russia and the PGE deposits of the Bushveld Complex, their modeling indicates that PGE-rich magmas could be a result of a multistage upgrading process with dissolution of FeS of pre-existing sulfide through its interaction with successive S-undersaturated magmas (Kerr and Leitch, 2005).

The unusually high PGE concentrations in the small Jinbaoshan sill support a model of either PGE-enriched sulfide entrainment or unusually PGE-rich magmas. The model of PGE-enriched sulfide entrainment may not be suitable for Jinbaoshan because such a model cannot answer why PGE-poor layers also display the primitive mantle-normalized chalcophile element patterns enriched PGE relative to Ni and Cu. A more likely model to interpret the PGE enrichment of all the rocks at Jinbaoshan that is they formed from PGE-rich magma. The approach of Kerr and Leitch (2005) is adopted in this study to model the compositions of sulfide liquid of the Jinbaoshan sill. The assumptions of the model are that (1) an initial mass of sulfide liquid M^0_{sulf} with initial metal concentration X_0 interacts with N successive batches of silicate magmas also with metal concentration X_0, (2) the incremental R-factor (R'_{inc}), mass of a magma pulse that first comes into the system compared with the mass of contacted sulfide liquid, should be a constant, and (3) a fraction L of the sulfide liquid dissolves into the magma after an interaction between the new magma pulse and residual sulfide liquid. The metal concentration in the last remaining sulfide liquid ($X^N_{sulfide}$) can be calculated using the equation (Kerr and Leitch, 2005):

$$\frac{X^N_{sulfide}}{X_0}=\left(\frac{DR'_{inc}}{R'_{inc}-LD}\right)\times\left[1-\left(\frac{D}{R'_{inc}+D-LD}\right)^N\right]$$

The cumulative R-factor (R_{cum}) that means a cumulative mass of silicate magma passing through the system compared with the mass of sulfide liquid at the Nth step can be expressed as (Kerr and Leitch, 2005):

$$R_{cum}=\frac{R'_{inc}}{L}\left[\left(\frac{1}{1-L}\right)^N-1\right]$$

Fraction of remaining sulfide liquid ($f_{sulfide}$) after N steps can be calculated using equation (Kerr and Leitch, 2005):

$$f_{sulfide}=\frac{R'_{inc}/L}{R'_{inc}/L+R_{cum}}$$

Modeling results (Table 3) indicate that the multistage-dissolution upgrading gave a reasonable fit to the compositions of sulfide liquid at Jinbaoshan. Assuming that $D_{Ni}=500$, $L=0.02$, and $R'_{inc}=100$, Ni concentration in sulfide liquid reaches 8.0% at $R_{cum}=3120$ and stabilizes at ~8.1% at $R_{cum}>\sim12{,}000$. Given $D_{Cu}=600$, Cu concentration in sulfide liquid reaches 3.9% at $R_{cum}=3120$ and increases slowly to 4.1% at $R_{cum}=\sim12{,}000$. If an uncertainty of ±10% is considered, these values are consistent with the observed average Ni and Cu contents calculated to 100% sulfide for the rocks of PGE-rich layers at

Jinbaoshan (Table 3). The constant Ni and Cu concentrations after R_{cum} = ~12,000 indicate that higher R_{cum} values have essentially no effect on Ni and Cu concentrations in sulfide liquid once they stabilize at a certain R_{cum} value. On the other hand, the observed Pt concentration of 112 ppm at 100% sulfide requires a R_{cum} of 14,356 if D_{Pt} = 10,000 (Table 3). At R_{cum} = 14,356, Pd concentration is 75 ppm at D_{Pd} = 6000, and 129 ppm at D_{Pd} = 40,000, both are lower than the observed Pd value of 147 ppm at 100% sulfide. The modeled Pd value agrees well with the observed value at R_{cum} = 16,414 when D_{Pd} = 40,000, and the modeled Pt value of 124 ppm at R_{cum} = 16,414 is also within the reasonable range of 10% uncertainty (Table 3). Therefore, the modeling results indicate that multistage-dissolution upgrading is a possible way to produce high PGE concentrations of the rocks at Jinbaoshan.

Note that all the partition coefficients selected in this modeling are within the range of PGE partition coefficients listed by Barnes and Lightfoot (2005), the results are therefore thought to be reasonable. The modeling indicates that PGE behavior is different from Cu and Ni and that PGE concentrations in sulfide liquid generally increase without limits during advanced dissolution, whereas Ni and Cu concentrations in sulfide liquid stabilize at certain R_{cum} value. Therefore, the Cu/Pd ratios of the sulfide liquid decrease during advanced dissolution and range from 5000 to 270.

The modeling results also indicate that 23% of the original sulfide liquid remained in the system at R_{cum} = 16,414. If later S-undersaturated magma pulse dissolved all the remaining PGE-rich sulfide liquid, the magma itself would become PGE-enriched relative to Cu and Ni. Therefore, the low Cu content of magmas is also part of the reason for low Cu/Pd and Cu/Zr ratios of the rocks at Jinbaoshan. Low Cu/Zr ratio therefore cannot be used as an indicator of sulfide removal from the magma at Jinbaoshan. Caution is therefore advised in the use of this ratio to infer overall mineral potential in similar cases.

6.6. A model for the formation of the Jinbaoshan sill and its PGE horizons

The formation of the Jinbaoshan sill involved an open system of magma conduit (Fig. 11). Early S-undersaturated magma pulses may have reached sulfide saturation due to fractionation of olivine and chromite and resulted in immiscible sulfide liquid segregated in a deep-seated staging magma chamber. The sulfide saturation was also likely triggered by crustal contamination as previous studies have indicated that variable degrees of crustal contamination were effective to trigger immiscible sulfide melts in staging magma chambers during the formation of Ni–Cu-dominated, sulfide-rich deposits elsewhere in the ELIP, such as the Baimazhai and Limahe deposits (Wang and Zhou, 2006; Tao et al., 2008). The staging magma chamber subsequently became a magma conduit for later magma incursions (① in Fig. 11). Successive pulses of S-undersaturated magma passing through the staging chamber stirred up the sulfide liquid and upgraded the sulfide in PGE along with dissolving some of the sulfide. Consequently, the sulfide liquid would decrease in mass and remaining sulfide liquid would become enriched in PGE. The remaining PGE-rich sulfide liquid would be pushed out and trapped by a later pulse of magma toward an upper magma chamber at higher level.

The PGE-rich sulfide liquid trapped in the silicate magma could be dissolved in the magma on the way up to the upper magma chamber with the decease of pressure as S-solubility may increase during the ascent of the magma along the conduit with decreasing pressure (Mavrogenes and O'Neill, 1999). The magma that dissolved the PGE-rich sulfide liquid would become PGE-rich (② in Fig. 11).

When the PGE-rich magma entered into the upper magma chamber, large amount of chromite crystallization may trigger sulfide saturation. Chromite and sulfide may settle along with olivine towards the base of the magma chamber. Dense chromite accumulated at the bottom of the magma chamber due to their high density

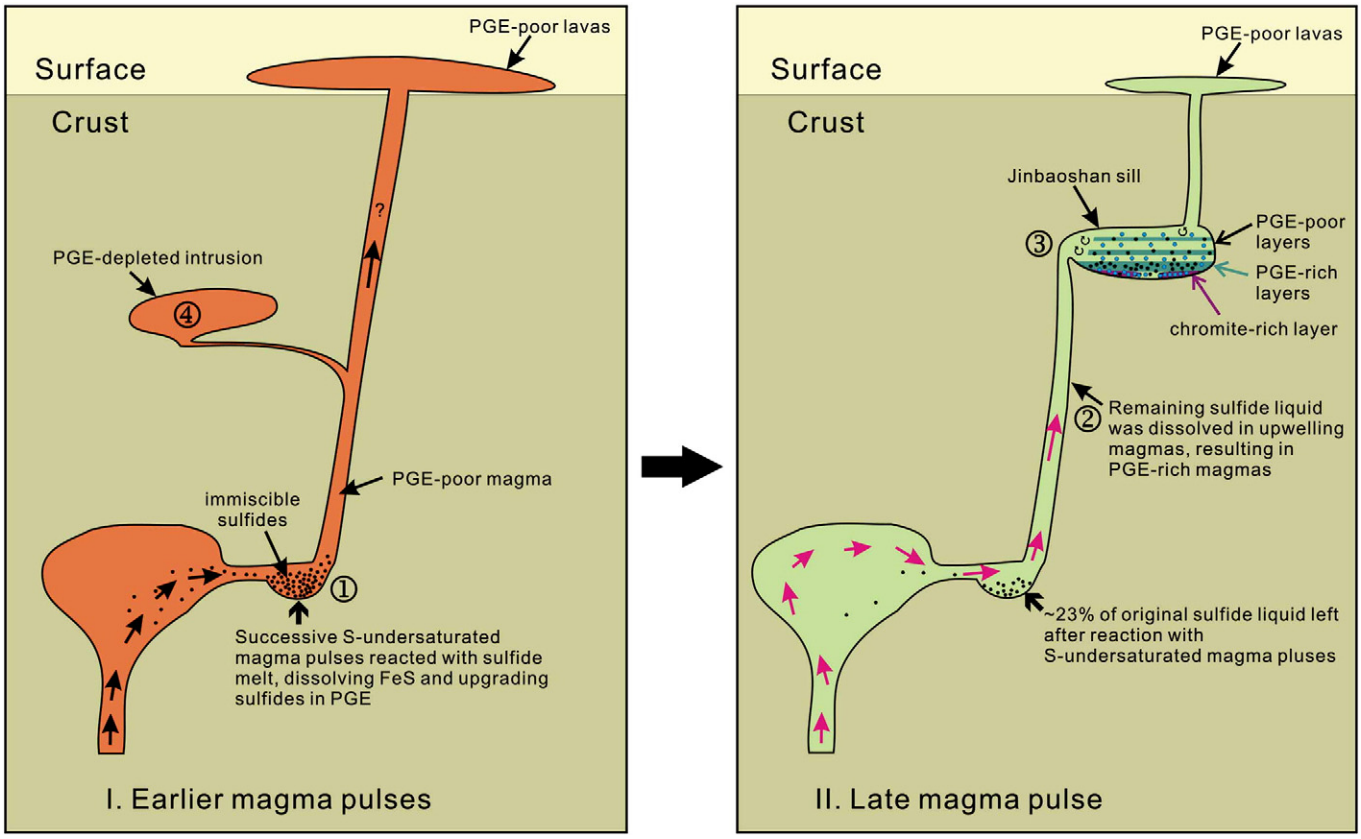

Fig. 11. A schematic model showing the formation of the Jinbaoshan sill.

relative to sulfide and the magma from which they crystallized so that the chromite-rich sulfide-poor layer at the bottom is overlain by PGE-rich sulfide-rich Layer I (③ in Fig. 11).

After large proportion of chromite and sulfide liquid settled at the base of magma chamber, minor suspending sulfide liquid was located at PGE-rich layer III and PGE-rich layer V by turbulence and convection within the magma chamber. Given the two distinct trends shown in the plots of metal versus S (Fig. 7), the turbulence and convection may be caused by a new PGE-magma pulse, which may also allow the suspending sulfide liquid access to more silicate liquid, so that the sulfide liquid with the highest PGE concentrations and large *R*-factor (e.g., Fig. 10) was present in the magmas from which the PGE-rich Layer III formed. The fact that sulfide contents of layers II to VI are substantially lower than those for Layer I also supports the settling and sorting of sulfide in the magma chamber. Except for Layer I, only a few samples with >0.5% sulfide are confined in Layers III and V, which is comparable with well-known examples of igneous layering produced by crystal sorting, such as those in the Duke Island Complex, Alaska (Irvine, 1974) and the Skaergaard intrusion, Greenland (Wager and Brown, 1968; Irvine et al., 1998).

The composition of the Jinbaoshan sill does not represent that of the parental magma because the MgO contents of the rocks are 20 to 40%. Textural relationship that the chromite and sulfide phases are always interstitial to olivine indicates that fractionation of sulfide and chromite was later than olivine crystallization. Therefore, the magma could have been emplaced into the upper magma chamber as an olivine-bearing crystal mush. Alternatively, the fractionated silicate liquid may have been squeezed out after magma was emplaced, presumably by tectonic events. The squeezed fractionated magmas might form intrusive and/or volcanic rocks with PGE characteristics being like PGE-poor layers. In addition, the earlier magma pulses that reacted with sulfide liquid at deep-seated magma chamber would become depleted in PGE to form PGE-depleted intrusive and/or volcanic rocks elsewhere (④ in Fig. 11). If these had happened, the intrusions and volcanic lavas elsewhere in this region could have PGE concentrations variable from PGE-rich to PGE-depleted. However, this conclusion needs to be confirmed by examining the PGE distribution of the ELIP basalts in this region.

7. Conclusions

The Jinbaoshan sill provides a very good example of high grade PGE deposit that formed from PGE-rich magmas in a magma conduit system. The PGE-rich magmas were generated by S-understaurated magmas dissolving PGE-rich sulfide liquid. The sulfide liquid was upgraded by a multistage-dissolution upgrading process in a deep-seated magma chamber, i.e., successive pulses of S-undersaturated magma that passed through the staging chamber upgraded the sulfide in PGE along with dissolving some of the sulfide. Large amounts of chromite crystallization triggered sulfide saturation of PGE-rich magmas in the upper magma chamber. PGE-rich layers in different stratigraphic heights resulted from settling and sorting of sulfide aided by turbulence and convections within the magma chamber.

Acknowledgements

This study was supported by a CAS Project No. KZCX2-YW-Q04-06 to CYW, the Hundred Talent Program of the Chinese Academy of Sciences to CYW and LQ, the CAS/SAFEA International Partnership Program for Creative Research Teams (KZCX2-YW-t004) and a Chinese 973 project matching grant from HKU. Zongyong Zhang and Jingdong Qi from Yunbao Mining Company at Jinbaoshan are thanked for providing great assistance during the field work at Jinbaoshan. Critical and very constructive comments from three reviewers, Wolfgang Maier, Sarah-Jean Barnes and an anonymous reviewer, are appreciated. This is contribution No. IS-1222 from GIGCAS.

Appendix A. Blank, detection limits and analytical results of reference materials

Standards	S	Ni	Ir (ppb)	Ru (ppb)	Rh (ppb)	Pt (ppb)	Pd (ppb)
UMT-1(expected)*			8.8	10.9	9.5	128	106
UMT-1 (this study)			7.03	9.51	8.86	107	104
WPR-1 (expected)*			13.5	22	13.4	285	235
WPR-1 (this study)			12.9	23.4	12.9	342	228
WMS-1 (expected) *			235	99	225	1741	1185
WMS-1 (this study)			210	89	198	1714	984
DZE-1 (expected) **	510	2500					
DZE-1 (this study)	492	2836					
Blank			0.0025	0.0017	0.0026	0.018	0.037
Detection limits			0.002	0.002	0.002	0.013	0.022

*Govindaraju (1994); **DZE-1: ultramafic rock.

Appendix B. Supplementary data

Supplementary data to this article can be found online at doi:10.1016/j.lithos.2010.07.022.

References

Barnes, S.J., Fiorentini, M.L., 2008. Iridium, ruthenium and rhodium in komatiites: evidence for iridium alloy saturation. Chemical Geology 257, 44–58.
Barnes, S.-J., Lightfoot, P.C., 2005. Formation of magmatic nickel sulfide ore deposits and processes affacting their copper and platinum-group contents. Economic Geology 100th Anniversary Volume, pp. 173–213.
Barnes, S.-J., Maier, W.D., 1999. The fractionation of Ni, Cu and the noble metals in silicate and sulfide liquids. In: Keays, R.R., Lesher, C.M., Lightfoot, P.C., Farrow, C.E.G. (Eds.), Dynamic Processes in Magmatic Ore Deposits and their Application to Mineral Exploration: Geological Association of Canada Short Course Notes, 13, pp. 69–106.
Barnes, S.-J., Maier, W.D., 2002. Platinum-group elements and microstructures of normal Merensky Reef from Impala Platinum Mines, Bushveld Complex. Journal of Petrology 43, 103–128.
Barnes, S.-J., Naldrett, A.J., 1986. Geochemistry of the J-M (Howland) Reef of the Stillwater Complex, Minneapolis adit area. II Silicate mineral chemistry and petrogenesis. Journal of Petrology 27, 791–825.
Barnes, S.J., Tang, Z.L., 1999. Chrome spinels from the Jinchuan Ni–Cu sulphide deposit, Gansu Province, People's Republic of China. Economic Geology 94, 343–356.
Barnes, S.-J., Naldrett, A.J., Gorton, M.P., 1985. The origin of the fractionation of platinum-group elements in terrestrial magmas. Chemical Geology 53, 303–323.
Barnes, S.-J., Couture, J.-F., Sawyer, E.W., Bouchaib, C., 1993. Nickel–copper occurrences in the Belleterre–Angliers belt of the Pontiac subprovince and the use of Cu–Pd ratios in interpreting platinum-group element distributions. Economic Geology 88, 1402–1418.
Barnes, S.J., Hill, R.E.T., Perring, C.S., Dowling, S.E., 1999. Komatiite flow-fields and associated Ni-sulphide mineralization, with examples from the Yilgarn block. Geological Association of Can Short Course Notes 13, 159–195.
Bezmen, N.I., Asif, M., Brugmann, G.E., Romanenko, I.M., Naldrett, A.J., 1994. Distribution of palladium, rhodium, ruthenium, iridium, osmium and gold between sulphide and silicate melts. Geochimica et Cosmochimica Acta 58, 1251–1260.
Campell, I.H., Naldrett, A.J., 1979. The influence of silicate:sulphide ratios on the geochemistry of magmatic sulfides. Economic Geology 74, 1503–1505.
Capobianco, C.J., Drake, M.J., 1990. Partitioning of ruthenium, rhodium and palladium between spinel and silicate melt. Geochimica et Cosmochimica Acta 54, 869–874.
Cawthorn, R.G., 2005. Pressure fluctuations and formation of the PGE-rich Merensky and chromitite reefs, Bushveld Complex. Mineralium Deposita 40, 231–235.
Chai, G., Naldrett, A.J., 1992a. The Jinchuan ultramafic intrusion: cumulate of a high-Mg basaltic magma. Journal of Petrology 33, 277–303.
Chai, G., Naldrett, A.J., 1992b. Characteristics of Ni–Cu–PGE mineralisation and genesis of the Jinchuan deposit, Northwest China. Economic Geology 87, 1475–1495.
Chung, S.L., Jahn, B.M., 1995. Plume–lithosphere interaction in generation of the Emeishan flood basalts at the Permian–Triassic boundary. Geology 23, 889–892.
Fleet, M.E., Crocket, J.H., Stones, W.E., 1996. Partitioning of platinum-group elements (OS, Ir, Ru, Pt, Pd) and gold between sulfide liquid and basalt melt. Geochimica et Cosmochimica Acta 60, 2397–2412.
Gauert, C.D.K., de Waal, S.A., Wallmach, T., 1995. Geology of the ultrabasic to basic Uitkomst Complex, eastern Transvaal, South Africa: an overview. Journal of African Earth Science 21, 553–570.
Godel, B., Barnes, S.-J., Maier, W.D., 2007. Platinum-group elements in sulphide minerals, platinum-group minerals, and whole-rocks of the Merensky Reef (Bushveld Complex, South Africa): implications for the formation of the reef. Journal of Petrology 48, 1569–1604.
Govindaraju, K., 1994. Compilation of working values and sample description for 383 geostandards. Geostandard Newsletter 18, 1–158.
Irvine, T.N., 1974. Petrology of the Duke Island ultramafic complex, southeastern Alaska. Geological Society of American Memoirs 138, 240.

Irvine, T.N., 1977. Origin of chromitite layers in the Muskox intrusion and other stratiform intrusions: a new interpretation. Geology 5, 273–277.
Irvine, T.N., Andersen, J.C.Ø., Brooks, C.K., 1998. Included blocks (and blocks within blocks) in the Skaergaard intrusion: Geologic relations and the origins of rhythmic modally graded layers. Geological Society of American Bulletin 110, 1398–1447.
Jugo, P.J., Luth, R.W., Richards, J.P., 2005. An experimental study of the sulfur content in basaltic melts saturated with immiscible sulfide or sulfate Liquids at 1300 °C and 1.0 GPa. Journal of Petrology 46, 783–798.
Keays, R.R., Nickel, E.H., Groves, D.I., McGoldrick, P.J., 1982. Iridium and palladium as discriminants of volcanic-exhalative, hydrothermal, and magmatic nickel sulfide mineralization. Economic Geology 77, 1535–1547.
Kerr, A., 2001. The calculation and use of sulfide metal contents in the study of magmatic ore deposits: a methodological analysis. Exploration and Mining Geology 10, 289–301.
Kerr, A., Leitch, A.M., 2005. Self-destructive sulfide segregation systems and the formation of high-grade magmatic ore deposits. Economic Geology 100, 311–332.
Kinnaird, J.A., Kruger, F.J., Nex, P.A.M., Cawthorn, R.G., 2002. Chromitite formation — a key to understanding processes of platinum enrichment. In: Mcdonald, I., Gunn, A.G., Prichard, H.M. (Eds.), 21st century Pt–Pd deposits: current and future potential: Transaction of Institute Mining and Metallurgy Section B: Applied earth science, 111, pp. 23–35.
Kruger, F.J., Kinnaird, J.A., Nex, P.A.M., Cawthorn, R.G., 2002. Chromite is the key to PGE. 9th International Platinum Sympium. Stillwater, U.S.A. pp. 211–213.
Lesher, C.M., 1989. Komatiite-associated nickel sulfide deposits. Review Economic Geology 4, 45–101.
Lesher, C.M., Campbell, I.H., 1993. Geochemical and fluid-dynamic modeling of compositional variations in Archean komatiite-hosted nickel sulfide ores in Western Australia. Economic Geology 88, 804–816.
Li, C., Naldrett, A.J., 1999. Geology and petrology of the Voisey's Bay intrusion: reaction of olivine with sulphide and silicate liquids. Lithos 47, 1–31.
Li, C., Maier, W.D., de Waal, S.A., 2001. Magmatic Ni–Cu versus PGE deposits: contrasting genetic controls and exploration implications. South African Journal of Geology 104, 309–318.
Li, C., Ripley, E.M., Maier, W.D., Gomwe, T.E.S., 2002. Olivine and sulfur isotopic compositions of the Uitkomst Ni–Cu sulfide ore-bearing complex, South Africa: Evidence for sulfur contamination and multiple magma emplacements. Chemical Geology 188, 149–159.
Lightfoot, P.C., Hawkesworth, C.J., 1997. Flood basalts and magmatic Ni, Cu and PGE sulphide mineralization: comparative geochemistry of the Noril'sk (Siberian traps) and West Greenland sequences. American Geophysical Union Monograph 100, 357–380.
Lightfoot, P.C., Keays, R.R., 2005. Siderophile and chalcophile metal variations in flood basalts from the Siberian Trap, Noril'sk Region: implications for the origin of the Ni–Cu–PGE sulfide ores. Economic Geology 100, 439–462.
Maier, W.D., 2005. Platinum-group element (PGE) deposits and occurrences: mineralization styles, genetic concepts, and exploration criteria. Journal of African Earth Science 41, 165–191.
Maier, W.D., Barnes, S.-J., 1999. Platinum-group elements in silicate rocks of the Lower, Critical and Main Zones at Union section, western Bushveld Complex. Journal of Petrology 40, 1647–1671.
Maier, W.D., Li, C., de Waal, S.A., 2001. Why are there no major Ni–Cu sulfide deposits in large layered mafic–ultramafic intrusions? Canadian Mineralogist 39, 547–556.
Mavrogenes, J.A., O'Neill, H.C., 1999. The relative effects of pressure, temperature and oxygen fugacity on the solubility of sulfide in mafic magmas. Geochimica et Cosmochimica Acta 63, 1173–1180.
Mungall, J.E., 2002. Kinetic controls on the partitioning of trace elements between silicate and sulfide liquids. Journal of Petrology 43, 749–768.
Naldrett, A.J., 1999. World class Ni–Cu–Co deposits: key factors in their genesis. Mineralium Deposita 34, 227–240.
Naldrett, A.J., 2004. Magmatic Sulphide Deposit: Geology, Geochemistry and Exploration. Springer, Heidelberg Berlin New York.
Naldrett, A.J., Lightfoot, P.C., 1999. Ni–Cu–PGE deposits of the Noril'sk region, Siberia: their formation in conduits for flood-basalt volcanism. Geological Association of Canada Short Course Notes 13, 195–249.
Naldrett, A.J., von Gruenewaldt, G., 1989. Association of platinum group elements with chromite in layered intrusions and ophiolite complexes. Economic Geology 84, 180–187.
Naldrett, A.J., Fedorenko, V.A., Lightfoot, P.C., Kunilov, V.I., Gorbachev, N.S., Doherty, W., Johan, Z., 1995. Ni–Cu–PGE deposits of the Noril'sk region, Siberia: their formation in conduits for flood basalt volcanism. Transactions of Institute Mining and Metallurgy 104B, 1–86.
Naldrett, A.J., Fedorenko, V.A., Asif, M., Lin, S., Kunilov, V.I., Stekhin, A.I., Lightfoot, P.C., Gorbachev, N.S., 1996. Controls on the composition of Ni–Cu sulfide deposits as illustrated by those at Noril'sk, Siberia. Economic Geology 91, 751–773.
Naldrett, A.J., Asif, M., Krstic, S., Li, C., 2000. The composition of ore at theVoisey's Bay Ni–Cu sulfide deposit, with special reference to platinum-group elements. Economic Geology 95, 845–866.
Naldrett, A.J., Wilson, A., Kinnaird, J., Chunnett, G., 2009. PGE tenor and metal ratios within and below the Merensky Reef, Bushveld Complex: implications for its genesis. Journal of Petrology 50, 625–659.
Page, N.J., Zientek, M.L., Czamanske, G.K., 1985. Sulfide mineralization in the Stillwater Complex and underlying rocks. In: Czamanske, G.K., Zientek, M.L. (Eds.), Stillwater Complex: Montana Bureau of Mines and Geology, Specical Publication, No. 92, pp. 93–96.
Peach, C.L., Mathez, E.A., Keays, R.R., Reeves, S.J., 1994. Experimentally determined sulfide melt-silicate melt partition coefficients for iridium and palladium. Chemical Geology 117, 361–377.
Peck, D.C., Keays, R.R., 1990. Insights into the behaviour of precious metals in primitive, S-undersaturated magmas: evidence from the Heazlewood River complex, Tasmania. Canadian Mineralogist 28, 553–577.
Qi, L., Zhou, M.-F., 2008. Determination of platinum-group elements in OPY-1: comparison of results using different digestion techniques. Geostandands and Geoanalytical Research 32, 377–387.
Qi, L., Hu, J., Gregoire, D.C., 2000. Determination of trace elements in granites by inductively coupled plasma mass spectrometry. Talanta 51, 507–513.
Qi, L., Zhou, M.-F., Wang, C.Y., 2004. Determination of low concentrations of platinum group elements in geological samples by ID-ICP-MS. Journal of Analytical Atomic Spectrometry 19, 1335–1339.
Qi, L., Zhou, M.-F., Wang, C.Y., Sun, M., 2007. Evaluation of the determination of Re and PGEs abundance of geological samples by ICP-MS coupled with a modified Carius tube digestion at different temperatures. Geochemical Journal 41, 407–414.
Song, X.Y., Zhou, M.-F., Tao, Y., Xiao, J.F., 2008. Controls on the metal compositions of magmatic sulfide deposits in the Emeishan large igneous province, SW China. Chemical Geology 253, 38–49.
Stockman, H.W., Hlava, P.F., 1984. Platinum group minerals in alpine chromitites from southwestern Oregon. Economic Geology 79, 491–508.
Tao, Y., Li, C., Hu, R., Ripley, E.M., Du, A., Zhong, H., 2007. Petrogenesis of the Pt–Pd mineralized Jinbaoshan ultramafic intrusion in the Permian Emeishan Large Igneous Province, SW China. Contributions to Mineralogy and Petrology 153, 321–337.
Tao, Y., Li, C., Song, X.Y., Ripley, E.M., 2008. Mineralogical, petrological, and geochemical studies of the Limahe mafic–ultramafic intrusion and associated Ni–Cu sulfide ores, SW China. Mineralium Deposita 43, 849–972.
Tao, Y., Ma, Y.S., Miao, L.C., Zhu, F.L., 2009. SHRIMP U–Pb zircon age of the Jinbaoshan ultramafic intrusion, Yunnan Province, SW China. Chinese Science Bulletin 54, 168–172.
Teigler, B., Eales, H.V., 1993. Correlation between chromite composition and PGE mineralization in the Critical Zone of the western limb of the Bushveld Complex. Mineralium Deposita 28, 291–302.
Tredoux, M., Lindsay, N.M., Davies, G., McDonald, I., 1995. The fractionation of platinum group elements in magmatic systems, with the suggestion of a novel causal mechanism. South African Journal of Geology 98, 157–167.
Von Gruenewaldt, G., Hatton, C.J., Merkle, R.K.W., 1986. Platinum-group element–chromitite associations in the Bushveld Complex. Economic Geology 81, 1067–1079.
Wager, L.R., Brown, G.M., 1968. Layered Igneous Rocks. Oliver and Boyd, Edinburgh. 588 pp.
Wang, C.Y., Zhou, M.-F., 2006. Genesis of the Permian Baimazhai magmatic Ni–Cu–(PGE) sulfide deposit, Yunnan, SW China. Mineralium Deposita 41, 771–783.
Wang, C.Y., Zhou, M.-F., Zhao, D.G., 2005. Mineral chemistry of chromite from the Permian Jinbaoshan Pt–Pd–sulphide-bearing ultamafic intrusion in SW China with petrogenetic implications. Lithos 83, 47–66.
Wang, C.Y., Zhou, M.-F., Qi, L., 2007. Permian flood basalts and mafic intrusions in the Jinping (SW China)–Song Da (northern Vietnam) district: mantle sources, crustal contamination and sulfide segregation. Chemical Geology 243, 317–343.
Wang, C.Y., Prichard, H.Z., Zhou, M.-F., Fisher, P.C., 2008. Platinum-group minerals from the Jinbaoshan Pd–Pt deposit, SW China: evidence for magmatic origin and hydrothermal alteration. Mineralium Deposita 43, 791–803.
Wilson, A.H., Chunnett, G.C., 2007. Trace element and platinum group element distributions and the genesis of the Merensky Reef, Western Bushveld Complex, South Africa. Journal of Petrology 47, 2369–2403.
Xu, Y.G., Chung, S.-L., Jahn, B.M., Wu, G.Y., 2001. Petrologic and geochemical constraints on the petrogenesis of Permian–Triassic Emeishan flood basalts in southwestern China. Lithos 58, 145–168.
Zhang, Z.C., Mahoney, J.J., Mao, J.W., Wang, F.S., 2006. Geochemistry of picritic and associated basalt flows of the western Emeishan flood basalt province, China. Journal of Petrology 47, 1997–2019.
Zhou, M.-F., 1994. PGE distribution in 2.7-Ga layered komatiite flows from the Belingwe greenstone belt, Zimbabwe. Chemical Geology 118, 155–172.
Zhou, M.-F., Yang, Z.X., Song, X.Y., Lesher, C.M., Keays, R.R., 2002a. Magmatic Ni–Cu–(PGE) sulphide deposits in China. In: Cabri, L.J. (Ed.), The Geology, Geochemistry, Mineralogy, Mineral Beneficiation of the Platinum-Group Elements: Canadian Institute of Mining, Metallurgy and Petroleum Specical, vol. 54, pp. 619–636.
Zhou, M.-F., Malpas, J., Song, X.Y., Kennedy, A.K., Robinson, P.T., Sun, M., Lesher, C.M., Keays, R.R., 2002b. A temporal link between the Emeishan large igneous province (SW China) and the end-Guadalupian mass extinction. Earth and Planetary Science Letter 196, 113–122.
Zhou, M.-F., Arndt, N.T., Malpas, J., Wang, C.Y., Kennedy, A.K., 2008. Two magma series and associated ore deposit types in the Permian Emeishan large igneous province, SW China. Lithos 103, 352–368.